Layered convection and the impacts of the perovskite-postperovskite phase transition on mantle dynamics under isochemical conditions

M. H. Shahnas[1] and W. R. Peltier[1]

Received 10 December 2009; revised 22 June 2010; accepted 12 July 2010; published 17 November 2010.

[1] The issue of the style of the mantle convection process remains important to the understanding of Earth's deep interior and surface processes. While results from structural seismology may be interpreted to support the existence of a whole mantle convection regime, in several geographic regions high-resolution reconstructions of Benioff zone body wave heterogeneity demonstrate that the downgoing slab appears to be "trapped" in the transition zone rather than continuing to penetrate unimpeded into the lower mantle. The presence of the recently discovered exothermic perovskite-postperovskite (Pv-pPv) phase transition that appears to define the top of the D'' layer adjacent to the core-mantle boundary may be expected to exert considerable impact on the mixing process. On the basis of the use of the most recent mantle parameters derived on the basis of mineral physics and a viscosity model inferred from glacial isostatic adjustment and Earth rotation observables, we reinvestigate the impact of the Pv-pPv transition on mantle mixing. Our analyses are based on a newly constructed axisymmetric control volume model, which is described in detail. Analyses with this model demonstrate that the action of the Pv-pPv transitions slightly decreases the tendency to layered flow due to the endothermic transitions that occur at 660 km depth and enhances the absolute radial mass flux especially in the lower mantle. However, the results also demonstrate that the episodically layered style of mantle mixing persists in models in which the strength of the Pv-pPv transition is significant.

Citation: Shahnas, M. H., and W. R. Peltier (2010), Layered convection and the impacts of the perovskite-postperovskite phase transition on mantle dynamics under isochemical conditions, *J. Geophys. Res.*, *115*, B11408, doi:10.1029/2009JB007199.

1. Introduction: The Continuing Debate Concerning the Style of Mantle Mixing

[2] The dynamical state of Earth's mantle is of fundamental importance to the understanding of surficial features, continental drift and plate tectonics, Earth's thermochemical history, and maintenance of the planetary magnetic field against ohmic dissipation. If convective mixing is whole mantle in style, the only thermal boundary layers that would exist within its volume would be those adjacent to Earth's surface and to the core-mantle boundary [e.g., *Peltier*, 1980; *Davies and Richards*, 1992; *Jordan et al.*, 1993]. On the other hand, if the convective circulation were layered, then an internal thermal boundary layer would exist across the interface separating the individually convecting regions [e.g., *Peltier*, 1996]. Despite intensive effort over the past several decades, there has been no definitive resolution of the debate concerning the relative merits of these alternative views.

[3] While early numerical work suggested that the Clapeyron slope of the endothermic phase transition horizon at 660 km depth was insufficiently negative to induce a layered style of flow [*Christensen and Yuen*, 1984, 1985], later analyses performed using improved models of this influence delivered results that were suggestive of a more important impact [*Peltier and Solheim*, 1992]. In this work, the Clapeyron slope assumed for this transition (−2.8 MPa/K) was based on the early experimental evidence of *Ito and Takahashi* [1989]. In the more recent literature, this value of the Clapeyron slope has been challenged, and values as low as −1.3 MPa/K have been suggested [*Fei et al.*, 2004; *Katsura et al.*, 2003]. However, it has also been established experimentally that, at pressures between 20 and 30 GPa, a series of phase transitions from spinel + stishovite through ilmenite also occur in the upper mantle near the depth of the 660 km horizon. The experimental work of *Kato et al.* [1995], for example, demonstrated that spinel + stishovite transforms into ilmenite at ~20.0 GPa, and that ilmenite itself transforms into perovskite at ~24.0 GPa at 800°C. The ilmenite-perovskite transition has a more negative Clapeyron slope than that of the spinel-perovskite + magnesiowustite transition, which was the focus of the earliest work, and this additional physics may also be important to the mixing process.

[4] High-resolution seismic tomographic imaging has established that, although some subducting slabs do even-

[1]Department of Physics, University of Toronto, Toronto, Ontario, Canada.

0148-0227/10/2009JB007199

tually sink into the lower mantle, there are nevertheless regions in which the slabs are strongly inhibited in their vertical descent by physical processes occurring at the base of the transition region near 660 km depth [*van der Hilst et al.*, 1991; *Fukao et al.*, 1992; *Zhao*, 2004; *Deal and Nolet*, 1999; *Creager and Jordan*, 1986]. On the basis of a new approach (grid parameterization) applied to a large data set of ISC (International Seismological Center) travel times, whole mantle *P* wave tomographic inversion [*Zhao*, 2004] has revealed the existence of more intense and broader high-velocity anomalies than previously observed at transition zone depths beneath regions of subduction, suggesting that slab material is rendered stagnant in a number of geographical regions before finally penetrating into the lower mantle. The descending slabs of lithosphere in the Western Pacific tend to be of this type, and the slabs which eventually descend into the lower mantle seem not to retain their original identity below the 660 km discontinuity [*Fukao et al.*, 1992].

[5] The tomographic sections of *P* wave anomalies beneath northeast China and central Japan and those of the Farallon subduction zone [*Zhao*, 2004] reveal that in both cases slab stagnation occurs at the 660 km depth horizon, and detached slab material is seen beneath this level in the lower mantle. In the case of the subducted Farallon plate, a large amount of slab material has accumulated in the transition zone due to the inhibition of its penetration into the lower mantle [*Schmid et al.*, 2002]. Inspection of the tomographic cross sections of the Kuril slab, Japan slab, and Izu-Bonin slab [*Deal and Nolet*, 1999] show that in the case of the Kuril slab there is an extension of the slab that extends horizontally along the endothermic phase transition boundary. In the northern region of Japan, there exists an indication of slab penetration into the lower mantle; however, the slab is nevertheless significantly deflected at the 660 km horizon, and there are regions in which the downwelling slab lies flat along the 660 km interface. Although there does exist evidence of penetration of the Izu slab into the lower mantle, a large volume of slab material between the endothermic transition at 660 km depth and the exothermic olivine-spinel transition at 410 km depth appears to be stagnating above the endothermic horizon.

[6] *Peltier and Solheim* [1992] and *Solheim and Peltier* [1994a, 1994b], based on their analysis of the impact of the endothermic transition on mantle mixing, which showed this to be highly episodic, argued in favor of the view that this style of mantle convection was required to understand the observational evidence. This view was reinforced by *Stein and Hofmann* [1994] from a chemical geodynamics perspective. The totality of the observational evidence reviewed above was suggested to be consistent with phase transition induced layered convection in which episodes of no or low mass transfer between the lower and upper mantle were followed by relatively brief episodes of whole mantle convective mixing. Histograms of the variation through time of the rate of crust formation demonstrate that the periods of rapid crust formation alternate with quiescent periods of low crust production [*Dearnley*, 1965; *Hong et al.*, 2004] (see *Peltier et al.* [1997] for a reproduction of Dearnley's results). In the interpretation of such data, *Peltier et al.* [1997] argued that this episodicity in the irreversible differentiation of the mantle to produce continental crust is intimately connected to the so-called Wilson cycle of supercontinent creation and destruction.

[7] The higher values of the ratio ^{3}He/^{4}He [*Lupton and Craig*, 1975; *Krylov et al.*, 1974] in deep mantle derived sources (oceanic island basalts; OIB) compared to those characteristic of midoceanic ridge basalts (MORB) source material suggests the existence of a relatively isolated lower mantle reservoir for the nonradiogenic helium that has been present since Earth formation. This interpretation remains somewhat controversial, however, as some [e.g., *Anderson*, 1998] interpret the high ratio of ^{3}He/^{4}He in OIB source material to be a consequence of mixing because of a deficiency in radiogenic ^{4}He compared with that characteristic of MORB samples.

[8] Analyses of the ^{40}Ar budget, however, support the existence of dynamical mantle layering [*Allegre et al.*, 1996]. The ^{40}Ar in the Earth is almost entirely the product of ^{40}K decay, and unlike helium, which can easily escape from the Earth's atmosphere because of its low mass, argon has been retained since the formation of the Earth. *Allegre et al.* [1996] have argued, on the basis of the amount of argon residing in Earth's atmosphere [*Turekian*, 1959] and in the Earth's crust, that an amount of argon in the range of 63×10^{18} to 80×10^{18} g should reside elsewhere in the interior of the Earth. A concentration of 500 ppm K content is required if the missing argon is assumed to reside in the core. However, this is outside the bounds of estimates based on the composition of chondritic material. Furthermore the rare gases favor coexistence with a silicate phase rather than with metals [*Matsuda et al.*, 1993]. A two-layer model in which the missing argon resides in mantle with a concentration of 230 ppm [*Allegre et al.*, 1996] in the lower mantle requires that little or no exchange of mass has occurred between the lower mantle and the overlaying region since Earth formation. However, other analyses of the ^{40}Ar budgets do not insist that the data require a little degassed lower mantle but rather permit the existence of a lower mantle that is only slightly less degassed than the upper mantle [e.g., *Davies*, 1999]. This latter interpretation of the argon budget is consistent with the episodically layered model of convective mixing.

[9] These argon and helium data, taken together with the direct seismological evidence, therefore support the episodically layered or partially layered convection models [e.g., *Peltier and Solheim*, 1992; *Solheim and Peltier*, 1993, 1994a, 1994b; *Peltier et al.*, 1997].

[10] Our primary interest in this paper is in the question as to whether this model remains robust from a dynamical perspective given the evidence that has recently been forthcoming for the existence of a further exothermic phase transformation that appears to define the top of the *D″* layer adjacent to the CMB.

2. The Perovskite-PostPerovskite Transition: A New Contribution to the Mantle Mixing Process

[11] The existence of a layer with distinct properties near the CMB was first recognized by *Dahm* [1934] as reviewed by *Peltier* [2007]. However, it was *Bullen* [1950] who named the layer *D″* and noted that it was characterized by significant laterally varying topography and complexity of its internal velocity structure. Since that time significant effort has

been expended in the attempt to more fully understand this enigmatic feature of the deep Earth. When interpreted simply as a thermal boundary layer, this region is believed to be the origin of mantle plumes [e.g., *Lay*, 2005], which are envisioned as arising through boundary layer instability [*Yuen and Peltier*, 1980]. A discontinuous and intermittent increase in seismic wave velocities in the region within 200–300 km of the core-mantle boundary has been reported in several regions [e.g., *Garnero and Lay*, 2003; *Lay et al.*, 2004]. Furthermore, a travel time triplication has been attributed to a sharp velocity discontinuity (~2%–3% in magnitude) in the same region near the base of mantle. Early modeling work of *Lay and Helmberger* [1983] based on construction of synthetic seismograms indicated a triplication, which is reproduced by the assumption of a 2.75% ± 0.25% shear velocity increase about 280 km above the core-mantle boundary. Some such triplications are strong and easily detectable, whereas others are weak and equivocal. Several of these locations are found in areas of the CMB that lie directly beneath the surface locations of previous subduction zones. The CMB region beneath Central America is a good example. The tomographic images beneath Central and North America obtained by the 3-D inverse scattering of core-reflected shear waves were interpreted as a post-perovskite lens about 2300 km wide and 250 km thick [*van der Hilst et al.*, 2007], and the internal D'' stratification may reflect multiple phase boundary crossings. Other examples appear to be located beneath surface hot spots as is the case of with the areas of the CMB beneath the South Atlantic Ocean and beneath the Central Pacific Ocean, above which sublithospheric subduction has not occurred in the recent past. Whereas in the upper mantle and most of the lower mantle, the variations of shear and bulk sound velocities ($v_s = (\mu/\rho)^{1/2}$, $v_\phi = (K/\rho)^{1/2}$, respectively) are well correlated; in the deepest lower mantle, they are poorly correlated and most often are in fact anticorrelated [*Su and Dziewonski*, 1997]. This observation cannot be explained in terms of the temperature dependence of these parameters since, for pure thermal heterogeneity, δv_s and δv_ϕ would be well correlated. Furthermore, thermal variations alone are also unable to explain the high values of the Poisson ratio ($\nu = -\varepsilon_{trans}/\varepsilon_{axial}$, where ε_{trans} and ε_{axial} are transverse and axial strains, respectively) in the deep mantle [*Mao et al.*, 2006].

[12] The primary composition of Earth's lower mantle is believed to be (Mg, Fe)SiO_3 perovskite, with lesser amounts of ferropericlase (Mg,Fe)O and $CaSiO_3$ [*Fiquet*, 2001]. However, this mineralogy cannot explain the unusual properties of the lowermost ~250 km of the mantle, which is commonly accepted to be the source of deep mantle plumes. Under lower mantle conditions, $MgSiO_3$ perovskite was initially expected to be stable [*Fiquet et al.*, 2000; *Serghiou et al.*, 1998; *Shim et al.*, 2001; *Ono et al.*, 2004]. It had been suggested by some, however, that this composition might transform into the oxides [*Saxena et al.*, 1996]. Some authors have also proposed the existence of significant chemical heterogeneity in D'' [*Kennett et al.*, 1998]. These observations have also led some to propose models of D'' having not only chemically distinct properties but also involving partial melting [*Lay et al.*, 2004].

[13] It was the work of *Sidorin et al.* [1999] which initiated the discussion of an alternative interpretation of this spatially intermittent seismic discontinuity at the base of the mantle as being more reasonably explained by the occurrence of a new phase transition having a Clapeyron slope of approximately 6 MPa/K near the CMB. Recent theoretical and experimental evidence for the existence of this post-perovskite (pPv) phase of Mg SiO_3 in the Earth's D'' layer has since triggered an entirely new interpretation of the observed seismic anisotropy within the D'' region [e.g., *Oganov and Ono*, 2004]. Experimental results reported by *Murakami et al.* [2004] demonstrated that Mg SiO_3 perovskite does indeed transform into a new high-pressure phase at a pressure above 125 GPa at a temperature of 2500 K (190 km above CMB) with an increase in density of about 1%–1.2%. The strong seismic anisotropy below the D'' discontinuity may also be attributed to this post-perovskite phase, which possesses a SiO_6 octahedral structure. However, the threshold for the occurrence of this new deep mantle phase depends on the thermal state. On the basis of both recent experimental and theoretical analysis [*Oganov and Ono*, 2004], it has been conjectured that the D'' layer could not have existed early in Earth history, as a consequence of the higher mantle temperature that would have existed early in the thermal evolution of the planet, but rather must have developed at later time once the interior had cooled sufficiently so as to fall below the perovskite-postperovskite (Pv-pPv) transition temperatures at the pressures that define the CMB region. At the present stage of the cooling history, the Pv-pPv transition is expected to occur only in the lowest temperature regions within D''. This could explain the characteristics of the observed shear velocity discontinuity, which are such that the high-velocity lenses are found only in regions that are expected to be anomalously cold [e.g., *Monnereau and Yuen*, 2007, 2010]. The presence of a very low-viscosity post-perovskite lens or layer above the CMB would be expected to enhance the CMB heat flux in the cold slab regions and may cause deflection of the cold subducting material in D'' [*Cizkova et al.*, 2010].

[14] On the basis of the S wave tomography model of *Grand* [2002] and assuming a Clapeyron slope of 6 MPa/K, *Helmberger et al.* [2005] obtained a thermally induced topographic map for the deep mantle transition boundary. This result suggests that the transition depth is shallower in the colder (higher velocity) regions and deeper in the hotter (lower velocity) regions. Therefore, one may expect a thicker D'' layer (consisting of pPv material) at locations where oceanic lithosphere has descended to the core-mantle boundary, thereby imposing a regional cold thermal anomaly. Similarly, in anomalously warm regions adjacent to the CMB, the postperovskite phase is expected to be absent. For a CMB temperature greater than the intercept temperature, which is the temperature of the phase transition at CMB pressure, there is a "double crossing" of the phase boundary by the geotherms associated with the cold descending flow [*Hernlund et al.*, 2005; *Monnereau and Yuen*, 2007]. Employing the seismic images of the D'' layer and double crossing depths, *Monnereau and Yuen* [2010] have attempted to put constraints on the CMB heat flux.

[15] Global seismic tomographic models have also revealed the existence of large-scale shear velocity anomalies in D'', with lower than the average velocity beneath the central Pacific, southern Africa, the southern Atlantic, and the south-

ern Indian Ocean. It has been proposed that two such large low-shear velocity provinces under the Pacific and Africa are also characterized by the presence of a compositional contribution to their velocity anomalies [*Lay et al.*, 2004]. Although the isochemical Pv-pPv phase transition increases the seismic velocities at the top of the D'' layer, the pPv phase itself, in interaction with the Earth's core, may absorb a significant amount of iron leading to an enhancement of the density increase, a reduction in the seismic velocities, and an increase in the Poisson ratio [*Mao et al.*, 2004, 2006]. Hotter regions at the base of the D'' layer in strong interaction with the outer core leads to enrichment of the iron content in ferromagnesian pPv silicate [*Mao et al.*, 2004] and significantly reduces seismic velocities, thus providing a possible explanation of the presence of ultra low velocity zones (ULVZ) above the CMB. The discovery of the pPv phase transition strongly suggests that it is most probably the correct explanation of the D'' layer, as it provides a satisfyingly parsimonious explanation of this enigmatic region, one that does not require the invocation of partial melt [*Lay et al.*, 2004] to explain such ULVZs.

[16] In the following sections of this paper, our purpose is to provide a systematic analysis of the impact of the presence of the Pv-pPv phase transition on mantle dynamics. Our analysis will be based on models that also include the additional phase transitions that occur at 410 and 660 km depth, which bracket the mantle transition zone that separates the upper mantle above 410 km from the lower mantle below a depth of 660 km. The new model we have developed as basis for these analyses is discussed in section 3.

3. A Multiphase Control Volume Formulation of Mantle Mixing

[17] The original model to be employed herein is based on the application of the control volume method [*Patankar*, 1980] to solve the basic hydrodynamic equations at high Prandtl number in axisymmetric spherical geometry. We have also developed a full 3-D model based on the same methodology but will employ the axisymmetric version of this model exclusively for present purposes. The axisymmetric results to be presented herein will be employed as basis for comparisons with the results from the 3-D models to be discussed elsewhere. The system of dynamical equations on which the model is based consist of conservation equations for mass (continuity), momentum, and internal energy which we solve for an anelastically compressible fluid with a proper equation of state that includes the olivine-spinel, spinel-Pv + magnesiowustite, and Pv-pPv phase transitions at 410, 660, and 2700 depth, respectively. The anelastic form of the continuity equation is

$$\nabla \cdot \left(\overline{\rho}\vec{V}\right) = 0, \tag{1}$$

in which $\overline{\rho}$ is the radial variation of density due to the self-compression of mantle material that defines the background state within which thermal convection exists. The infinite Prandtl number form of the expression for conservation of momentum is

$$-\nabla P + \nabla \cdot \overline{\overline{\sigma}} - \rho g\widehat{r} = 0. \tag{2}$$

The partial differential equation describing the conservation of internal energy is

$$C_P\overline{\rho}\frac{\mathrm{D}T}{\mathrm{D}t} - \alpha T\frac{\mathrm{D}P}{\mathrm{D}t} = \nabla \cdot (k\nabla T) + \Phi + \overline{\rho}H + \overline{\rho}l_i\frac{\mathrm{D}\Gamma_i}{\mathrm{D}t}. \tag{3}$$

The final relation that is required to close the system is the equation of state which we write in the form,

$$\rho = \overline{\rho}\left[1 - \alpha(T - T_{\mathrm{r}}) + \frac{1}{K_{\mathrm{T}}}(p - p_r)\right] + \Delta\rho_i(\Gamma_i - \Gamma_{ri}),\ i = 1, 2, 3, \tag{4}$$

where the deviatoric stress tensor is given by

$$\overline{\overline{\sigma}} = \eta\left[\nabla\vec{V} + \left(\nabla\vec{V}\right)^T\right] - \frac{2}{3}\eta\left(\nabla \cdot \vec{V}\right)\overline{\overline{I}}. \tag{5}$$

In this system of equations, ρ, g, α, T, T_{r}, V, p, η, C_{P}, k, K_{T}, and t denote density, gravitational acceleration, thermal expansion coefficient, temperature, reference temperature, velocity, pressure, dynamic viscosity in shear, heat capacity at constant pressure, thermal conductivity, bulk modulus at constant temperature, and time, respectively. $\Delta\rho_i$ is the density contrast between two solid phases at phase transition zone i, and Γ_i is a phase density functional defined by

$$\Gamma_i = \frac{1}{2}[1 + \tanh(\pi_i)], \tag{6}$$

where the nondimensional arguments of the hyperbolic tangent functions are given by

$$\pi_i = \frac{d_i - d - \gamma_i(T - T_i)}{h_i}. \tag{7}$$

d, d_i, h_i, T_i, and γ_i are depth, reference depth of phase boundary i, width of the ith divariant phase transition, transition temperature at the reference depth d_i, and the Clapeyron slope of the relevant phase transition, respectively. The quantity Φ in equation (3) represents the viscous dissipation rate per unit volume of the mantle flow. For spherical axisymmetric geometry, it has the following explicit form [*Solheim and Peltier*, 1994a],

$$\Phi = \eta\left\{2\left[\frac{\partial V_r}{\partial r}\right]^2 + 2\left[\frac{1}{r}\frac{\partial V_\theta}{\partial\theta} + \frac{V_r}{r}\right]^2 + 2\left[\frac{V_r}{r} + \frac{V_\theta\cot(\theta)}{r}\right]^2\right\} + \eta\left\{\left[\frac{\partial V_\theta}{\partial r} - \frac{V_\theta}{r} + \frac{1}{r}\frac{\partial V_r}{\partial\theta}\right]^2 - \frac{2}{3}\left[\nabla \cdot \vec{V}\right]^2\right\}. \tag{8}$$

We nondimensionalize the above system of equations based on the following scheme:

$$\begin{aligned} &r = r'\Delta r,\ T = T'\Delta T,\ \eta = \eta'\eta_0,\ k = k'k_0,\ \rho = \rho'\rho_0,\\ &C_{\mathrm{P}} = C'_{\mathrm{P}}C_0,\ g = g'g_0,\ \alpha = \alpha'\alpha_0,\ \kappa = \kappa'\kappa_0,\ t = t'\frac{d^2}{\kappa_0},\\ &p = p'\frac{\eta\kappa_0}{d^2},\ \sigma = \sigma'\frac{\eta\kappa_0}{d^2}, \end{aligned} \tag{9}$$

in which a zero subscript identifies a reference value; $\Delta r = R_{surf} - R_{CMB}$ and $\Delta T = T_{CMB} - T_{surf}$. The nondimensional momentum equation is then given by

$$-\nabla' P' + \nabla' \cdot \overline{\overline{\sigma}}' - R_0 \rho' g' \widehat{r} = 0, \tag{10}$$

where the Rayleigh number of the system is

$$R_0 \equiv \frac{g_0 \rho_0 d^3}{\eta_0 \kappa_0}. \tag{11}$$

Dropping the primes in order to simplify the notation then reduces equation (10) to

$$-\nabla P + \nabla \cdot \overline{\overline{\sigma}} - R_0 \rho g \widehat{r} = 0. \tag{12}$$

In the axisymmetric spherical formulation, we assume $\frac{\partial}{\partial \phi} = 0$ (longitudinal variation); therefore, the two components of the momentum equation are simply given by,

$$-\frac{\partial P}{\partial r} + \frac{1}{r^2}\frac{\partial}{\partial r}\left(r^2 \tau_{rr}\right) + \frac{1}{r\sin(\theta)}\frac{\partial}{\partial \theta}\left(\sin(\theta)\tau_{r\theta}\right) - \frac{\tau_{\theta\theta} + \tau_{\phi\phi}}{r} - R_0 \rho g = 0, \tag{13}$$

$$-\frac{1}{r}\frac{\partial P}{\partial \theta} + \frac{1}{r^2}\frac{\partial}{\partial r}\left(r^2 \tau_{r\theta}\right) + \frac{1}{r\sin(\theta)}\frac{\partial}{\partial \theta}\left(\sin(\theta)\tau_{\theta\theta}\right) + \frac{\tau_{r\theta}}{r} - \frac{\cot(\theta)}{r}\tau_{\phi\phi} = 0, \tag{14}$$

in which the nonzero tensor components are given by

$$\tau_{rr} = 2\eta \frac{\partial V_r}{\partial r} - \frac{2}{3}\eta\left(\nabla \cdot \vec{V}\right), \tag{15}$$

$$\tau_{\theta\theta} = 2\eta\left(\frac{V_r}{r} + \frac{1}{r}\frac{\partial V_\theta}{\partial \theta}\right) - \frac{2}{3}\eta\left(\nabla \cdot \vec{V}\right), \tag{16}$$

$$\tau_{\phi\phi} = 2\eta\left(\frac{V_r}{r} + \frac{V_\theta}{r}\cot(\theta)\right) - \frac{2}{3}\eta\left(\nabla \cdot \vec{V}\right), \tag{17}$$

$$\tau_{r\theta} = \tau_{\theta r} = \eta\left(\frac{\partial V_\theta}{\partial r} + \frac{1}{r}\frac{\partial V_r}{\partial \theta} - \frac{V_\theta}{r}\right). \tag{18}$$

In the control volume formulation, the spherical axisymmetric momentum equations (13) and (14) are integrated over the spherical volumes,

$$\Delta V = \frac{1}{3}\left(r_t^3 - r_b^3\right)\left(\cos(\theta_n) - \cos(\theta_s)\right), \tag{19}$$

for unit longitudinal angle ($\Delta\phi = 1$) [*Patankar*, 1980]. The subscripts t, b, n, and s stand for top, bottom, north, and south faces of the volume. We have made use of the SIMPLER scheme [*Patankar*, 1980] for the velocity-pressure iteration on a longitude-latitude grid. A staggered grid [*Patankar*, 1980; *Brandt*, 1982], in which the pressure is defined in the center of each cell and velocity components are defined at cell boundaries, has been used to avoid the occurrence of checkerboard pressure fields. This also has the advantage that all derivatives in the momentum and continuity equations involve adjacent points.

[18] The last term in the energy equation (3) is the contribution of the latent heat, which is released or absorbed at the phase transition horizon when material is transformed as it "flows through" the phase boundary. It can be shown that the total time derivative of Γ_i may be written in the form

$$\frac{D\Gamma_i}{Dt} = \alpha_i \frac{DT}{Dt} + \beta_i, \tag{20}$$

where

$$\alpha_i \equiv 2\Gamma_i(1-\Gamma_i)\frac{\gamma_i}{\left(\frac{dP}{dr}\right)_{r_i} h_i},$$
$$\beta_i \equiv -V_r \frac{2\Gamma_i(1-\Gamma_i)}{h_i}\left(1 + \frac{\gamma_i}{\left(\frac{dP}{dr}\right)_{r_i} h_i}\right). \tag{21}$$

The latent heat l_i is given by

$$l_i = \frac{\gamma_i \Delta\rho_i T}{\rho^2}. \tag{22}$$

The energy equation then takes the form

$$C_P \overline{\rho}\frac{DT}{Dt} + \alpha T \frac{DP}{Dt} = \nabla \cdot (k\nabla T) + \Phi + \overline{\rho}H + \left(\overline{\rho}\alpha_i \frac{DT}{Dt} + \overline{\rho}\beta_i\right) l_i. \tag{23}$$

Using the continuity equation, the first term in the energy equation may be written as

$$C_P \overline{\rho}\frac{DT}{Dt} = C_P\left[\frac{\partial}{\partial t}(\overline{\rho}T) + \nabla \cdot \left(\overline{\rho}T\vec{V}\right)\right]. \tag{24}$$

Ignoring time variation and lateral variation of the pressure, the adiabatic term in the energy equation may be approximated by

$$\alpha T \frac{DP}{Dt} \approx -\alpha \overline{\rho} g V_r T. \tag{25}$$

Putting all these together and rearranging terms, the energy equation is cast into the form:

$$(C_P - \alpha_i l_i)\left(\frac{\partial}{\partial t}(\overline{\rho}T) + \nabla \cdot (\overline{\rho}TV)\right) + \alpha T V_r \overline{\rho} g = \nabla \cdot (k\nabla T) + \Phi + \overline{\rho}H + \overline{\rho}\beta_i l_i. \tag{26}$$

In nondimensional form this becomes

$$(C_P' - \alpha_i' l_i')\left(\frac{\partial}{\partial t'}(\overline{\rho}'T') + \nabla' \cdot \left(\overline{\rho}'T'\vec{V}'\right)\right) + \xi_0 \alpha' T' V_r' \overline{\rho}' g' = \nabla' \cdot (k'\nabla' T') + \delta_0 \Phi' + \gamma_0 \overline{\rho}' H' + \omega_0 \overline{\rho}' \beta_i' l_i', \tag{27}$$

where

$$\xi_0 \equiv \frac{\alpha_0 g_0 d}{C_0},\ \delta_0 \equiv \frac{\eta_0 \kappa_0}{C_0 \rho_0 \Delta T d^2},\ \gamma_0 \equiv \frac{H_0 d^2}{C_0 \kappa_0 \Delta T},\ \omega_0 \equiv \frac{\eta_0 \kappa_0}{d^2 C_0 \rho_0 \Delta T}. \tag{28}$$

Dropping the primes, we have finally

$$(C_P - \alpha_i l_i)\left(\frac{\partial}{\partial t}(\overline{\rho}T) + \nabla\cdot\left(\overline{\rho}T\vec{V}\right)\right) + \xi_0\alpha T V_r \overline{\rho} g = \nabla\cdot(k\nabla T) + \delta_0\Phi + \gamma_0\overline{\rho}H + \omega_0\overline{\rho}\beta_i l_i \quad (29)$$

The energy equation is also integrated over the spherical control volume elements and in time. In compact form, we may then write

$$\int_{\Delta V}\int_t^{t+\Delta t}\frac{\partial T}{\partial t}\mathrm{d}t\mathrm{d}v = \int_{\Delta V}\int_t^{t+\Delta t} G(T)\mathrm{d}t\mathrm{d}v, \quad (30)$$

in which the function G includes all terms of equation (29), except for the partial time derivative of temperature. Integrating over volume and time, for each volume element we may write,

$$\left(T_P^1 - T_P^0\right)\Delta V = \left[\alpha G\left(T_P^1, T_N^1, T_S^1, T_B^1, T_T^1\right) + (1-\alpha)\cdot G\left(T_P^0, T_N^0, T_S^0, T_B^0, T_T^0\right)\right]\Delta t\Delta V,\ 0 \le \alpha \le 1. \quad (31)$$

The subscript P denotes the grid point at the center of the volume and N, S, B, and T stand for north, south, bottom, and top neighbor grid points. The superscripts 0 and 1 refer to the old value (known) and new value (unknown) of the temperature at time t and $t + \Delta t$, respectively. Here the weighting factor α [e.g., *Patankar*, 1980] enables us to have explicit solutions (α=0), fully implicit solutions (α=1), or semi-implicit solutions such as provided by the Crank-Nicolson scheme (α = 0.5) or an arbitrary semi-implicit scheme. However, in the present study, we have solely employed the explicit scheme.

[19] The energy equation at each grid point in the control volume formulation may then be rewritten in the form

$$a_P T_P = a_N T_N + a_S T_S + a_B T_B + a_T T_T + b, \quad (32)$$

where a_P, a_N, a_S, a_B, and a_T are the coefficients of the temperatures at the center of volume, north, south, bottom, and top neighbor grid points and b is the source term. The system of equation (32) is then solved using a power law scheme [*Patankar*, 1980], which suppresses unphysical variations in the temperature solution. In this formulation, we have

$$a_N = D_n A(|P_n|) + \left[[F_n, 0]\right], \quad (33a)$$

$$a_S = D_s A(|P_s|) + \left[[-F_s, 0]\right], \quad (33b)$$

$$a_B = D_b A(|P_b|) + \left[[F_b, 0]\right], \quad (33c)$$

$$a_T = D_t A(|P_t|) + \left[[-F_t, 0]\right], \quad (33d)$$

in which we have employed the notation $[[A, B]] \equiv \max(A, B)$, and

$$P \equiv \frac{\rho V d}{\kappa}(\text{Peclet number}), \quad (34a)$$

$$F \equiv \rho V(\text{mass flux}), \quad (34b)$$

$$D \equiv \frac{\kappa}{\delta x}(\text{diffusive conductance}), \quad (34c)$$

$$A(|P|) = \left[\left[0, (1 - 0.1|P|)^5\right]\right](\text{power law}). \quad (34d)$$

The lower case subscripts n, s, b, and t denote the quantity at the north, south, bottom, and top volume boundaries. Note that the $A(|P|) = 1$ limit represents the upwind advection scheme. The solution of the discretization equations are obtained using the tridiagonal-matrix algorithm (TDMA) as described by *Patankar* [1980]. The iterations are performed by sweeping the grid points in the radial and lateral directions alternatively. In order to take the effect of both boundary conditions into account (in each coordinate direction) on the discretized solutions, the grid points are swept back and forth in each iteration.

4. Thermodynamic Dependence of the Physical Properties

[20] In this section, we will provide a detailed description of the pressure and temperature dependence assumed for the physical properties of mantle material.

4.1. Thermal Expansivity

[21] The pressure- and temperature-dependent thermal expansion coefficient may be described by [e.g., *Fei*, 1995]

$$\alpha(p,T) = \alpha_0(T)\left(\frac{V(p,T)}{V(0,T)}\right)^{\delta_T}, \quad (35)$$

where δ_T is the Anderson-Gruneisen parameter and V represents the volume at pressure p and temperature T. The value of the thermal expansion coefficient may be calculated from equation (35), incorporating the third-order Birch-Murnaghan equation of state as

$$p = 3f(1+2f)^{5/2}K_{T_0}(T)\left[1 - \frac{3}{2}(4 - K'_{T_0})f\right], \quad (36)$$

where $K_{T_0}(T)$ is isothermal bulk modulus at zero pressure, K'_{T_0} is its pressure derivative, and the compression f is given by

$$f = \frac{1}{2}\left[\left(\frac{V(0,T)}{V(p,T)}\right)^{2/3} - 1\right]. \quad (37)$$

K'_{T_0} = 5.37 [*Fei*, 1995; *Schmeling et al.*, 2003] will be assumed for the purpose of all of the analysis to be discussed in this paper.

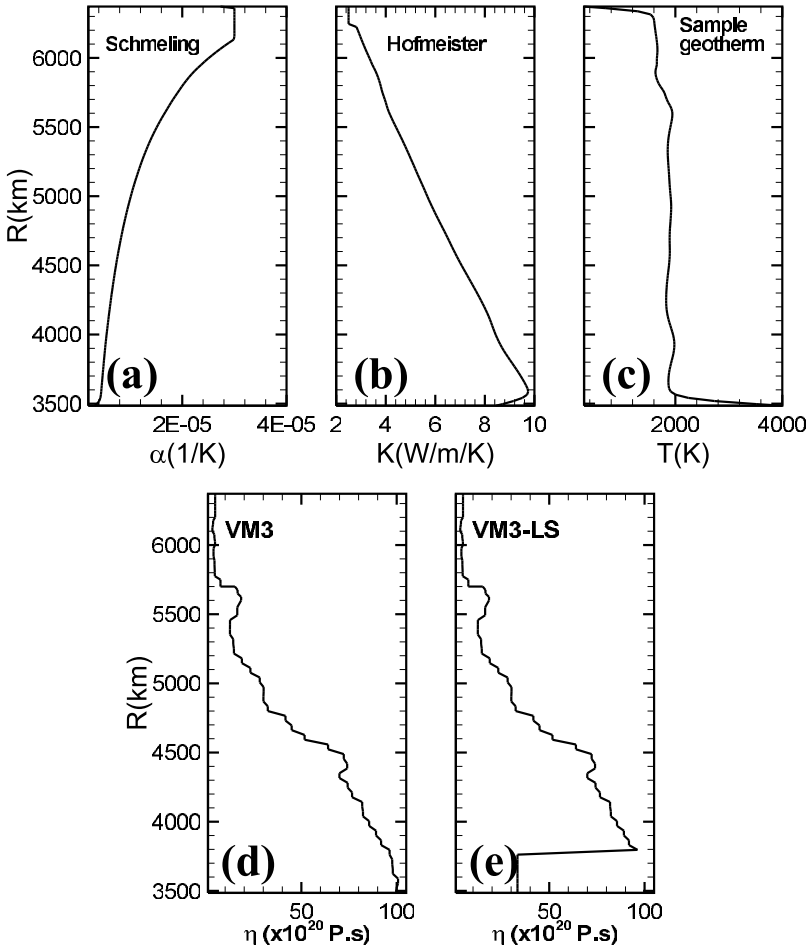

Figure 1. (a) Temperature- and pressure-dependent thermal expansivity [*Schmeling et al.*, 2003] and (b) temperature- and pressure-dependent thermal conductivity [*Hofmeister*, 1999] for (c) a sample geotherm, (d) VM3-vscosity profile [*Peltier*, 1998b], and (e) modified VM3-LS viscosity profile.

[22] For the temperature-dependent part of this coefficient, a power law relation which fits the experimental data over a specific temperature range [*Fei*, 1995] has been employed as

$$\alpha_0(T) = a_0 + a_1 T + a_2 T^{-2}. \tag{38}$$

The parameters for Forsterite are given by [*Fei*, 1995] as

$$a_0 = 3.034 \times 10^{-5}\ \mathrm{K}^{-1},\ a_1 = 7.422 \times 10^{-9}\ \mathrm{K}^{-2},$$
$$a_2 = -0.5381\ \mathrm{K}.$$

The temperature dependence of the bulk modulus may be obtained from the definition of the isothermal Anderson-Gruneisen parameter δ_T as

$$\delta_T = -\frac{1}{\alpha K_T}\left(\frac{\mathrm{d}K_T}{\mathrm{d}T}\right)_P. \tag{39}$$

For temperatures higher than the Debye temperature, δ_T and αK_T are almost independent of temperature. Using this approximation, equation (39) may be integrated [*Kumar*, 2000] to obtain

$$K_{T_0}(T) = K_0\left[1 - \alpha_0 \delta_T^0 (T - T_0)\right]. \tag{40}$$

The parameters for Forsterite are given by [*Fei*, 1995] as:

$$K_0 = 129\ \mathrm{GPa},\ \alpha_0 = 2.64 \times 10^{-5}\ \mathrm{K}^{-1},\ \delta_T^0 = 5.5,\ T_0 = 298\ \mathrm{K}.$$

Figure 1a displays the depth variation of this thermal expansion coefficient based on equation (35) for a sample geotherm (Figure 1c), which is restricted by assuming an upper limit of $3.0 \times 10^{-5}\ \mathrm{K}^{-1}$ on α near the surface. One important difference between the numerical models employed in this study and previous work [e.g., *Solheim and Peltier*, 1994a] is the lower value of the thermal expansivity assumed for the deepest mantle, particularly near the CMB, where low values of the thermal expansivity would otherwise tend to magnify the effect of the deep phase transition.

4.2. Thermal Conductivity

[23] In the present study, we will employ the pressure- and temperature-dependent thermal conductivity proposed by *Hofmeister* [1999] as

$$k(P,T) = k(298)\left(\frac{298}{T}\right)^a \exp\left[-\left(4\gamma + \frac{1}{3}\right)\int_{298}^{T} \alpha(\theta)\mathrm{d}\theta\right] \cdot \left(1 + \frac{K_0'}{K_0}\right) + \sum_0^3 b_i T^i. \tag{41}$$

The first and second terms in this semiempirical relation are the lattice vibration (phonon) and radiative transport (photon) contributions, respectively. The parameters are given by [*Hofmeister*, 1999; *van den Berg et al.*, 2002]

$$k(298) = 4.7\ \mathrm{Wm^{-1}K^{-1}},\ a = 0.3,\ \gamma = 1.2\ \mathrm{K},$$
$$K_0' = 5.37\ \mathrm{GPa},\ K_0 = 261\ \mathrm{GPa},$$
$$b_0 = 1.7530 \times 10^{-2},\ b_1 = -1.0365 \times 10^{-4},$$
$$b_2 = 2.2451 \times 10^{-7},\ b_3 = -3.4071 \times 10^{-11}.$$

Figure 1b displays the depth variation of this thermal conductivity for the sample geotherm (Figure 1c). The thermal conductivity has been restricted to a lowest value of 2.5 W m^{-1} K^{-1} near the surface.

4.3. Viscosity

[24] One of the most important parameters in any model of the mantle convection process is the viscosity of mantle material. The viscosity profile of the lower mantle, which has a major impact on inferences concerning the dynamics of convective mixing, is poorly known except on the basis of analysis of the glacial isostatic adjustment process [*Peltier*, 1998a; *Peltier and Drummond*, 2010]. The viscoelastic rebound of Earth's crust following a large-scale continental deglaciation event is recorded in local measurements of relative sea level history as well as a variety of modern geodetic measurements. Because the melting history of the ice sheets that existed during the most recent deglaciation event of the late quaternary ice age is well constrained, such rebound data may be formally inverted by Bayesian methods to obtain a well-constrained model of the depth variation of this quantity on the basis of a spherically symmetric parameterization.

[25] Shear wave splitting, which is the consequence of the existence of orthogonal polarizations of shear waves having different propagation speeds in passing through an anisotropic medium provides an additional means through which one may interrogate the stress-strain regime and constitutive relation for mantle material. However, in spite of the fact that (Mg,Fe)SiO_3 perovskite is characterized by significant elastic anisotropy, most of the lower mantle appears to have little or no anisotropy [*Silver et al.*, 1993], a fact that has led to this region of the deep Earth being referred to as existing in a superplastic regime [*Karato et al.*, 1995]. On the basis of high-temperature experimental results for an analog of perovskite having the same elastic constants as Mg SiO_3 perovskite, *Karato et al.* [1995] showed that, for reflected shear waves (ScS) from the CMB, the expected splitting for a rheology based on dislocation climb controlled creep would range from ~1 to ~36 s, and for the refracted shear wave (SKS) though the liquid core it would range from ~0.5 to ~18 s, depending on the geometry. However, the observed weak shear wave splitting, which is less than 0.2 s, indicates that the magnitude of the anisotropy in the lower mantle is less than ~1% of that of the upper mantle, which is most probably dislocation creep dominated. The rheology of olivine, the main constituent of the upper mantle, is a strong function of temperature, grain size, and stress [*Kirby*, 1983; *Poirier*, 1985; *Ranalli*, 1987, 1991] and power law creep is expected to be dominant for grain sizes larger than 1 mm at stresses higher than 1 MPa [*Ranalli*, 1991]. For the finer grain size expected to be characteristics of perovskite in the lower mantle, the rheology is expected to be dominated by diffusion creep and perovskite therefore to maintain an isotropic texture during deformation and recrystallization under lower mantle conditions. *Meade and Silver* [1995] and *Ito and Sato* [1991] have argued that the aseismicity in the lower mantle is the consequence of superplastic behavior of fine-grained material at moderately high temperatures and low strain rates (rheological weakening).

[26] Efforts have also been made to reconcile the radial structure of the mantle viscosity variation inferred on the basis of these two different approaches: namely the study of the expected physical properties of mantle material on the basis of laboratory experiments and the analysis of geoid and postglacial uplift observations combined with numerical models [*Peltier and Jiang*, 1997; *Forte et al.*, 1993; *Pari and Peltier*, 1995; *King*, 1995]. The radial viscosity structure to be employed in our models will be based on the viscosity models inferred from glacial isostatic adjustment observations [for recent reviews see *Peltier*, 1998b; *Peltier and Drummond*, 2010]. Such analyses combined with the Earth rotation observables related to the polar wander and nontidal acceleration of rotation processes suggest that in the deepest part of mantle the viscosity must be less than 1 order of magnitude higher than the viscosity of the upper mantle and transition zone [*Peltier and Jiang*, 1996; *Peltier and Drummond*, 2010].

5. Models to be Analyzed

[27] In order to analyze the impact of the phase transitions that bound the transition region as well as the newly discovered Pv-pPv transition on mantle dynamics and the degree of convective layering, we have employed the previously discussed control volume method which is able to accurately represent the conservation laws in circumstances in which sharp variations of physical properties occur such as across phase transition horizons. The most recent models for the temperature- and pressure-dependent thermal expansivity and thermal conductivity including both lattice and radiative contributions have been used. The significance of radiative conductivity on plume stabilization has been pointed out by *Matyska and Yuen* [2005] and *Yuen et al.* [2007]. In Cartesian numerical models, these authors showed that, in the absence of incorporation of the radiative contribution to conductivity and in models in which the thermal conductivity is assumed constant, the presence of the Pv-pPv phase transition enhances the time dependence of lower mantle convection. This results in the activation of a plethora of unstable lower mantle plumes which is not consistent with the few isolated plume clusters with large lateral dimensions that are observed to be present in the lower mantle [*Schubert et al.*, 2004]. In the results to be discussed in what follows we will illustrate the impact of the two radial viscosity profiles shown in Figure 1. One of these viscosity profiles is based directly on the results obtained through the analysis of isostatic adjustment observations, namely the VM3 viscosity model of *Peltier* [1998b] shown previously on Figure 1d. The second viscosity profile to be employed is one in which we have imposed a lower viscosity in the D'' layer below 2700 km depth [*Peltier and Drummond*, 2010]; hereafter, this model will be referred

Table 1. Time-Averaged (3 Gyr) Mantle Mean Temperature, Surface Heat Flow, Mass Flux Across the Exothermic Phase Boundary at 410 km Depth, Mass Flux Across the Endothermic Phase Boundary at 660 km Depth, and Mass Flux Across the Pv-pPv Phase Boundary at 2700 km Depth, for Model Sets 1 and 2 With 4000 K CMB Temperature and Model Sets 3 and 4 With 3600 K CMB Temperature

Model	T (K)	HF_Surf (TW)	MF_410 (kg/m^2/yr)	MF_660 (kg/m^2/yr)	MF_2700 (kg/m^2/yr)
Model Sets 1 and 2, CMB: 4000 K					
C00D00VM3	1607	51.0	37.8	30.4	15.4
C04D80VM3	1673	55.7	42.1	34.9	19.6
C08D80VM3	1710	56.9	42.7	36.1	21.2
C12D80VM3	1755	59.4	44.3	36.6	24.0
C16D80VM3	1787	60.8	44.5	36.9	26.4
C12D20VM3	1664	53.4	38.5	30.8	17.6
C12D40VM3	1687	55.9	40.4	33.3	20.5
C12D60VM3	1707	57.5	43.2	36.6	21.5
C00D00VM3-LS	1753	59.4	40.9	31.6	25.9
C04D80VM3-LS	1817	62.8	45.4	38.6	30.2
C08D80VM3-LS	1877	66.5	47.3	40.9	36.3
C12D80VM3-LS	1939	68.4	48.3	43.2	40.4
C16D80VM3-LS	1980	70.6	49.3	45.0	44.6
C12D20VM3-LS	1806	63.0	45.9	38.3	31.7
C12D40VM3-LS	1861	65.6	46.0	39.2	34.7
C12D60VM3-LS	1897	66.5	46.7	41.0	38.0
Model Sets 3 and 4, CMB: 3600 K					
C00D00VM3	1498	45.4	35.7	28.0	14.6
C04D80VM3	1566	48.8	37.7	30.1	18.1
C08D80VM3	1586	49.9	38.4	30.8	19.3
C12D80VM3	1606	51.6	39.9	33.7	22.4
C16D80VM3	1609	52.0	40.4	34.6	21.9
C12D20VM3	1541	47.8	38.3	31.7	17.4
C12D40VM3	1582	49.5	38.5	31.7	18.5
C12D60VM3	1607	51.5	40.6	33.5	21.0
C00D00VM3-LS	1627	53.0	40.3	32.1	24.8
C04D80VM3-LS	1695	56.1	42.4	35.8	30.0
C08D80VM3-LS	1725	58.1	43.8	37.0	33.1
C12D80VM3-LS	1762	60.2	45.2	40.5	37.7
C16D80VM3-LS	1789	61.3	46.7	40.6	40.0
C12D20VM3-LS	1681	55.0	41.0	32.2	28.3
C12D40VM3-LS	1719	57.2	43.2	38.2	31.7
C12D60VM3-LS	1746	58.5	44.6	38.7	35.0

to as employing the VM3-LS profile (Figure 1e). The viscosity in this narrow region is to be taken to be lower by a factor of 10 compared to the lower mantle viscosity characteristic of the VM3 profile. For the purpose of a few of the models to be employed, we have also used viscosity profiles with a stepwise increase at 660 km depth and the results delivered by these models will also be compared with those obtained using either VM3 or VM3-LS.

[28] The impact of the Pv-pPv phase transition on mantle dynamics has been investigated by employing four sets of numerical models. Because the mean depth of such phase transitions varies with temperature, the thermal state of Earth's mantle is clearly important to the degree of layering and may alter the dynamical influence of these transitions. In the first pair of sequences of numerical investigations we will assume a CMB temperature of 4000 K, whereas in the final two sequences the CMB temperature has been fixed to 3600 K [*Boehler*, 1992]; in both cases the surface temperature of the planet is fixed to 293 K. Sets 1 and 3 employ the VM3 viscosity profile, while sets 2 and 4 employ the VM3-LS profile. Comparison of the results obtained in these different model sequences will enable us to explore the impact of D'' viscosity on the dynamical influence of the mantle phase transitions. Table 1 provides a listing of the main models for which results have been obtained in the paper.

[29] A present-day internal heating rate of 13 TW (which is close to the requirement of Chondritic meteorites; see *Butler and Peltier* [2002] for discussion), which is uniformly distributed throughout the mantle, will be assumed for the purpose of all model analyses. At the external boundaries of the convecting mantle, the radial mass flux is assumed to vanish and free slip boundary conditions are imposed at both the CMB and surface. We will assume slopes of 3.0 and −3.0 MPa/K; together with the density contrasts of 200 and 440 kg/m^3 at the exothermic and endothermic phase transition boundaries at 410 and 660 km depth, respectively. Each of the four sets of numerical experiments includes eight models and involves two subsequences (Table 1). The first subsequence will include five models; the first in the sequence includes no pPv phase transition but the sequence continues with results for models with increasing Clapeyron slope ranging from 0 to 16 MPa/K. In this subset, excepting the first model which has no pPv phase transition, we fix the density contrast across the boundary to 80 kg/m^3. In the second subset which includes three models, we keep the Clapeyron slope for the pPv transition fixed to 12 MPa/K and vary the density contrast stepwise from 20 to 60 kg/m^3 (Table 1). These models span a range of density discontinuities and Clapeyron slopes that bracket the range of values suggested by both theoretical and experimental results. Our model nomenclature is such that each model name begins with the letter "C" representing the Clapeyron slope of the Pv-pPv transition and which is followed by two digits specifying the magnitude of the Clapeyron slope in MPa/K. This initial code is followed by the letter "D" and two digits specifying the density contrast across this transition in kg/m^3. Finally, the model name is terminated with either VM3 or VM3-LS specifying the viscosity profile employed (Figure 1). For example, in model C12D80VM3 the Clapeyron slope and density contrast of the Pv-pPv transition are 12 MPa/K and 80 kg/m^3, respectively, and the VM3 viscosity profile has been used. Model names for those employing step viscosity profiles end with "Step" followed by two digits specifying the magnitude of the viscosity contrast between the upper mantle and lower mantle. To explore the role of the magnitude of the Clapeyron slope of the endothermic phase transition at 660 km depth on layering we have also run models with different Clapeyron slopes. In these models, the model names end with "Endo," which is followed by two digits specifying the magnitude of the Clapeyron slope at the endothermic transition at 660 km depth in MPa/K.

[30] All models for which results are to be described in this paper were run until a statistically steady state was achieved such that no long-term trends in mean temperature, surface heat flow, or kinetic energy were observed. As discussed elsewhere [*Peltier and Solheim*, 1992; *Solheim and Peltier*, 1994a], the degree of layering of the flow is enhanced by increasing the Rayleigh number in the presence of the endothermic phase boundary. This is due to the greater vertical deflection of the phase boundary that is induced by the larger temperature gradients that persist across downwellings and upwellings in the high Rayleigh

number fluid. However, the degree of layering also depends on the thermal state of the mantle. As a quantitative diagnostic of the degree of layering, we will employ the modulus of the radial mass flux across the boundary as in the work of *Peltier and Solheim* [1992], namely,

$$F_m(r,t) = \frac{1}{S_r}\int_{S_r} \rho |V_r| \mathrm{d}s, \tag{42}$$

where the time-dependent average mass flux is evaluated over the spherical surface S_r at radius r. A plot of this absolute value of the mass flux provides a quantitative means by which to explore the degree of layering as a function of time. This is also an appropriate diagnostic of the effect of the Pv-pPv phase transition on mantle superplumes evaluated at the Pv-pPv phase transition level.

[31] The concept of weak post-perovskite lenses surrounded by relatively stiff perovskite plumes has been shown to be feasible by *Cizkova et al.* [2010] which may explain the viscosity paradox suggested by geoid inversion [*Cadek and Fleitout*, 2006]. On the basis of the recent inferences from theoretical studies and laboratory experiments on analogue post-perovskite material [*Hunt et al.*, 2009], one may expect that the rheology of post-perovskite would be dominated by the dislocation mechanism and therefore would be softer than perovskite. The large-scale lateral viscosity structure in the lowermost mantle reveals that the regions at the base of hot spots have significantly higher viscosity than the regions below subduction zones [*Yuen et al.*, 2007]. Furthermore, on the basis of the Earth rotation arguments, the lowermost part of the deep mantle could have significantly lower viscosity than in the overlaying region [*Peltier and Drummond*, 2010]. In order to take this into account, some of our numerical models include a low-viscosity layer adjacent to the CMB. All models include both the exothermic and endothermic phase transitions that bracket the mantle transition zone at the depth of 410 and 660 km, respectively. The results obtained for this sequence of models will provide a set of data that may be employed to investigate the influence of the Pv-pPv phase transition on the degree of layering as well as the influence of a possible low-viscosity zone near the CMB on mantle plumes in both the presence and absence of the Pv-pPv deep mantle phase transition. However, in order to determine how the variation in magnitude of the effective Clapeyron slope at the 660 km depth horizon may affect mantle layering, we assume the reference model denoted C00D00VM3, which has an effective Clapeyron slope of −3 MPa/K at 660 km depth and have included three additional models which differ from this model only in the magnitude of the effective slope of the combination of spinel-perovskite + magnesiowustite and ilmenite-perovskite phase transitions. The influence of the viscosity contrast between the upper and lower mantle has been investigated in a set of four models with viscosity contrasts of 5, 10, 20, and 50 between the transition zone and upper mantle and the lower mantle, and the results obtained from these models are also discussed in section 6.

6. Results

[32] A summary of results for the main models is presented in Table 1. The results obtained for the models with CMB temperature of 4000 K (set 1 and set 2) are summarized in the first part Table 1. In both of these sequences of models, the mean mantle temperature and the average surface heat flux are seen to increase with increase of either the Clapeyron slope of the Pv-pPv transition or the associated density jump across this deep mantle transition boundary. Similar effects have been reported by *Nakagawa and Tackley* [2004] using isochemical and anelastically compressible models in 2-D half-cylindrical geometry but with no internal heating. Time series of the average absolute mass fluxes at the horizon of the endothermic phase transitions at 660 km depth and that of the Pv-pPv phase transition at 2700 km depth for model set 1 are displayed in Figure 2. The influence of the deep mantle phase transition has been investigated using the models with different Pv-pPv transition parameters and are compared with the reference model C00D00MV3.

[33] Results for the models with constant density contrast but increasing Clapeyron slopes and constant Clapeyron slope but increasing density contrasts are compared with the model results for models with no Pv-pPv phase transition separately for clarity. Inspection of the results in Figure 2 will demonstrate that a sudden increase in mass flow at 660 km depth phase boundary is followed by a period during which the mass transfer between the upper mantle and lower mantle is low and the flow oscillates between these two states. Figures 2a and 2b show that the length scale characteristic of typical mantle avalanches decreases as either the Clapeyron slope of the Pv-pPv phase transition or the density jump across this transition boundary increases. In the models with higher deep mantle transition parameters, the average mass flux is higher and individual avalanches appear as sharp events characterized by intense transfers of mass between the upper mantle and the lower mantle. Similarly episodic mass flux events due in part to the episodic variation in dynamical pressure that is communicated to depth from the level of the endothermic phase transition are observed at the 2700 km depth horizon. Figures 2c and 2d show that the characteristic time scale of deep mantle mass flux events is less affected by the presence of the Pv-pPv phase transition, a fact that may be attributed to the higher viscosity of the deep mantle that is characteristic of the VM3 model. Layered mantle flow develops in periods during which the radial mass flux at 660 km depth is a minimum, and this condition causes the mantle temperature to decrease as the flow of heat across the CMB decreases.

[34] The time series of mass flux for the models with CMB temperature of 4000 K but which also include a low-viscosity D'' layer are displayed in Figure 3. Compared to the models with no deep mantle low-viscosity zone, it will be observed that the mantle avalanches in these models are more massive but less isolated in time and have similar characteristic length scales as those of the reference model C00D00VM3-LS and the average mass fluxes in these models are higher than their counterparts in the previously discussed sequence. Compared to the first set of models, the characteristic time scale of the mass flux events across the level of the deep mantle phase transition is significantly smaller in this second set of models but much enhanced in magnitude. Temporally averaged (3 Gyr) mantle mass flux time series provide an alternative way of investigating the

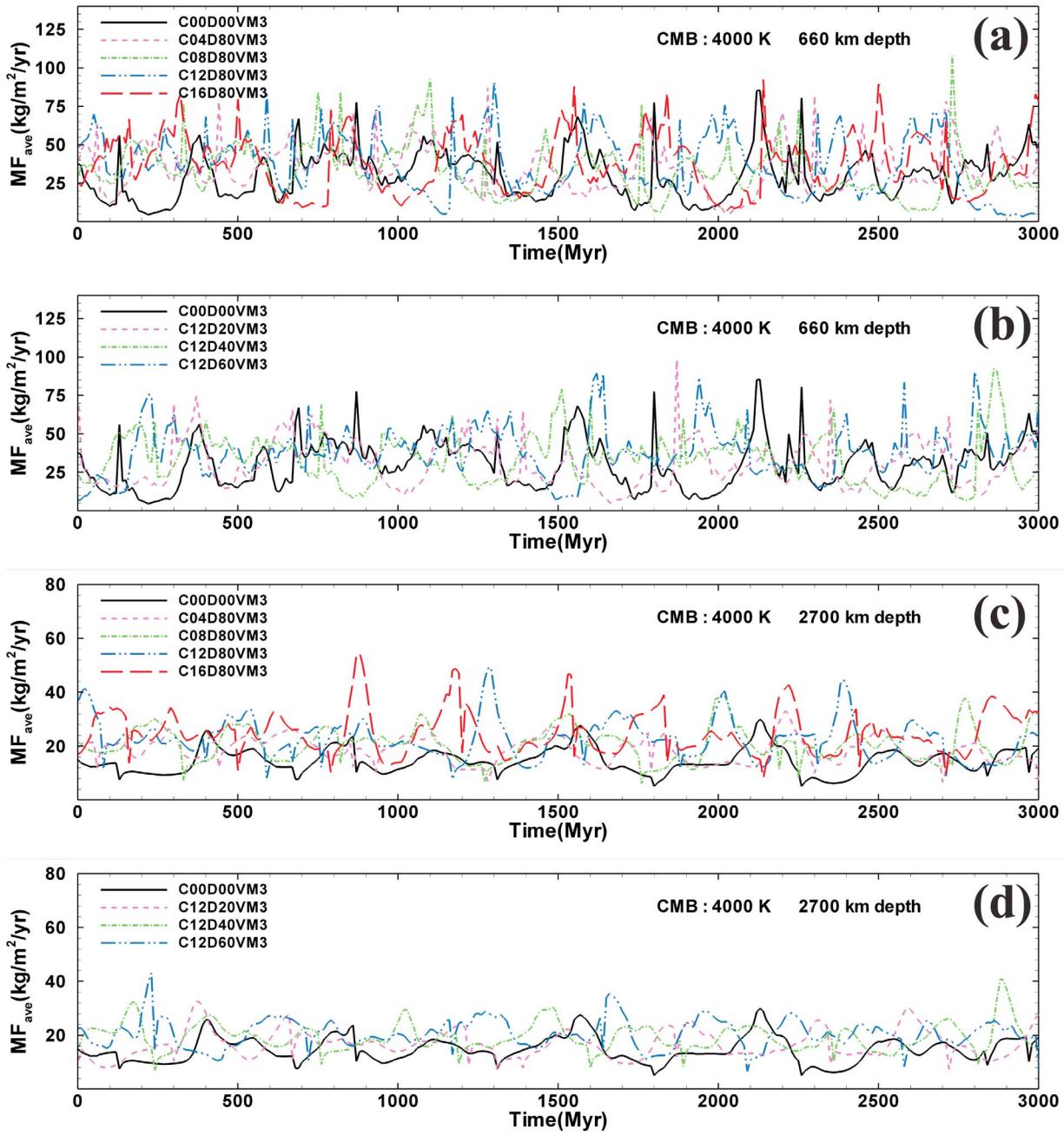

Figure 2. Time series of the mantle absolute mass flux across the 660 and 2700 km depth phase transition boundaries for the set of models with VM3 radial viscosity profile and CMB temperature of 4000 K.

style of mantle mixing. The time-averaged mass flux time series shown on Figure 4 provide a means of estimating the degree of layering in each model as well as the overall vigor of the circulation in the first two sets of models. Inspection of Figures 4a and 4c demonstrates that the increase in mass flux with and without the deep mantle low-viscosity zone is approximately 40% in the models with highest phase transition parameters. In all models mantle mixing increases with increasing values of the deep mantle phase transition parameters. The higher the values of these Clapeyron slopes and density increase parameters, the higher the mass flux. This is consistent with previous studies [e.g., *Nakagawa and Tackley*, 2004]; however, the persistence of the local minimum in radial mass flux at the depth of the endothermic transition in all models demonstrates that, although the mixing between the upper mantle and lower mantle increases and the degree of layering decreases, this tendency to layered flow never disappears. The second part of Table 1 summarizes the numerical results for model sequences 3 and 4, which include models similar to those of sets 1 and 2

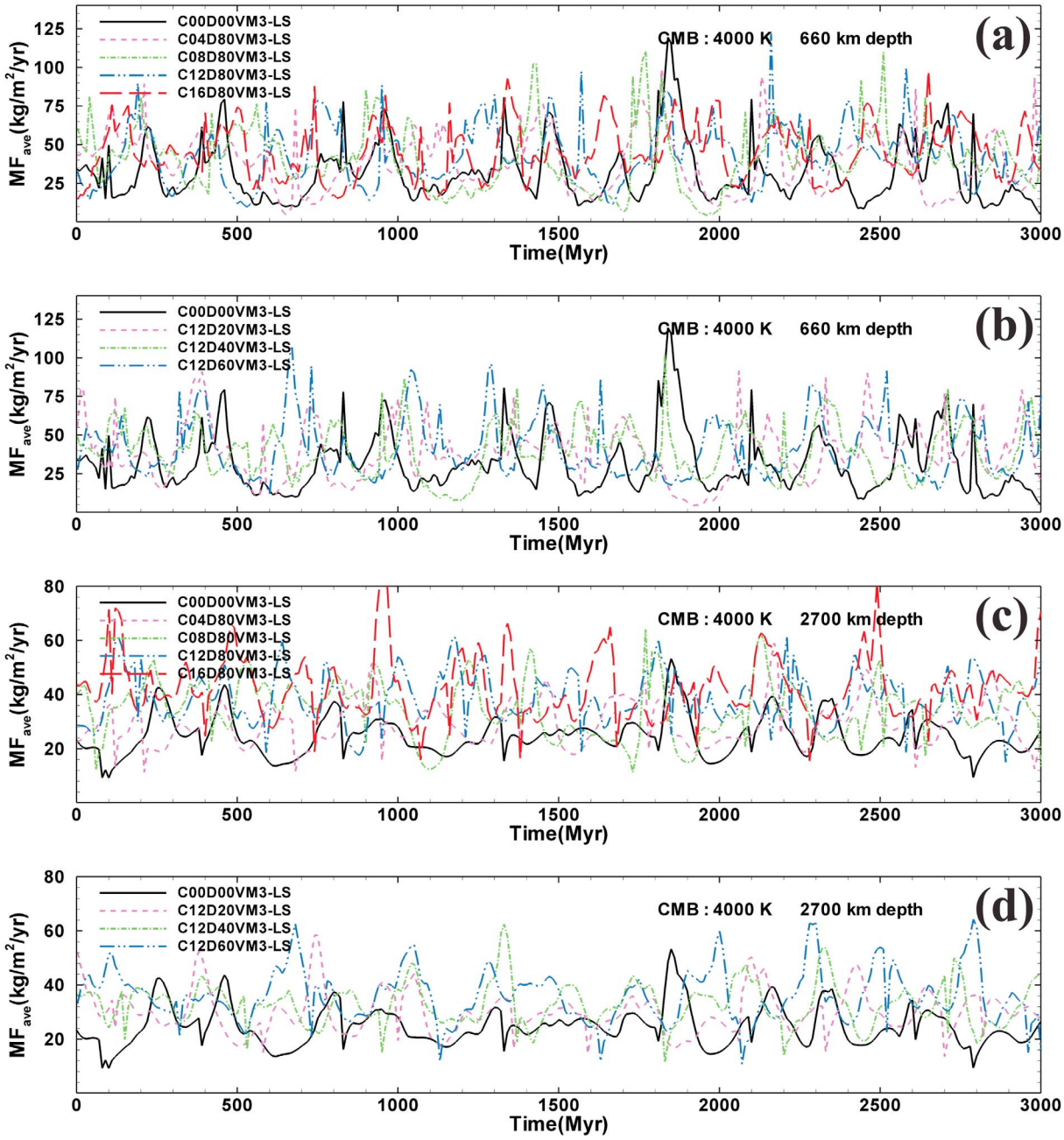

Figure 3. Time series of the mantle absolute mass flux across the 660 and 2700 km depth phase transition boundaries for the set of models with VM3-LS radial viscosity profile and CMB temperature of 4000 K.

but for which a CMB temperature of 3600 K has been assumed. The results are similar to those obtained for sets 1 and 2 except for the fact that there is a decrease in the intensity of all characteristics of the mixing process as would be expected.

[35] Snapshots of the circulation in model C00D00VM3 with CMB temperature of 4000 K after 3 Gyr of evolution are shown in Figures 5a–5f at 230, 390, 500, 1960, 2140, and 2360 Myr, respectively. In the initial frame, the mantle circulation is strongly layered with the remnants of a previously completed avalanche at 45° from the north, a state that is followed by two avalanche events and one plume penetration into the upper mantle that occur at a later time in Figure 5b. In Figure 5c, the circulation is almost entirely in a layered state. Similarly, the final three frames represent an avalanche event which is bracketed between two-layered states.

[36] Despite the fact that the effective Clapeyron slope at the level of the endothermic phase transition is not sufficiently steep to isolate the circulations on either side of this

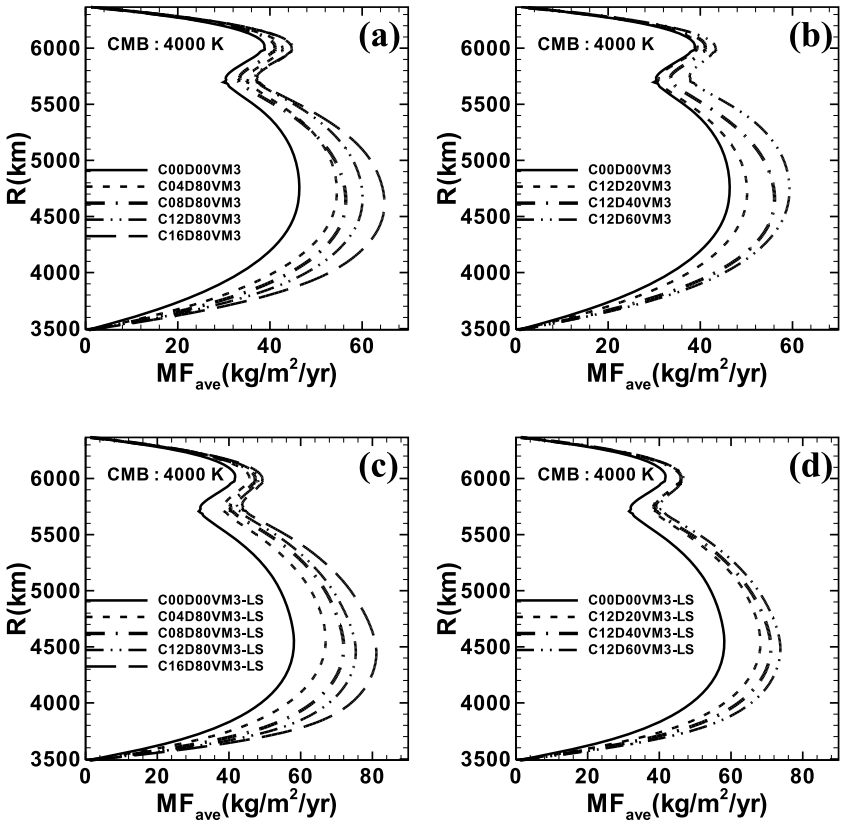

Figure 4. Temporally averaged (3 Gyr) absolute radial mass fluxes for the models with VM3 and VM3-LS viscosity profiles and CMB temperature at 4000 K.

horizon, it should be noted that there still may be regions during the time dependent evolution o the flow in which the horizontal component of the flow velocity is anticorrelated across the phase transition interface. Figure 6 displays three close-ups of the circulations demonstrating this fact. Figure 6a demonstrates that, although flow velocities on either side of the endothermic phase transition boundary (laterally extensive upper mantle circulation) are similar in magnitude, the temperature field suggests the upper mantle and lower mantle to be significantly isolated. Inspection of Figure 6b reveals that the small-scale circulations in the upper mantle are isolated from the lower mantle flow so that there are both parallel and antiparallel flow velocities at either side of the endothermic transition boundary. In Figure 6c, the flow velocities on the upper and lower sides of the transition boundary are essentially in the same direction. The flow velocity direction on either side of this phase transition boundary is affected by the degree of coupling between the upper and lower mantle, the vigor of the convection and surface instabilities. In the upper region of Figure 6a and the lower region of Figure 6b, there are downwellings in the upper mantle which lie horizontally above the 660 km discontinuity consistent with the seismological inferences discussed in section 1. In the latter case, there is also a folding in the mantle flow.

[37] Snapshots of temperature fields for the model set C16D80VM3 (Figures 7a–7c), C00D00VM3-LS (Figures 7d–7f), and C16D80VM3-LS (Figures 7g–7i) all with the CMB at 4000 K are shown in Figure 7. The first row displays snapshots at 780, 860, and 1020 Myr for the model C16D80VM3. Figure 7a represents a relatively layered mantle which is followed by Figure 7b after 80 Myr with two large avalanche events and one flow penetration into the upper mantle. After an additional 160 Myr (Figure 7c), the circulation is once more layered. The second row of graphics in Figure 7 displays snapshots of the temperature fields for C00D00VM3-LS at 320, 460, and 560 Myr for a model with almost whole mantle convection sandwiched between two-layered states. In the last row, we show snapshots from model C16D80VM3-LS at 820, 970, and 1100 Myr. It is evident that the inclusion of a low-viscosity zone in the deep mantle has increased the mean mantle temperature and the number of instabilities of the D'' layer about the core mantle boundary. These model results demonstrate that the layering persists in the presence of the Pv-pPv phase transition even with the highest transition parameters.

[38] The surface heat flux in all of the models described previously is either greater than or close to the upper bound of the observed modern surface heat flux at Earth's surface. This characteristic of the solutions is due primarily to the application of free slip boundary conditions at the surface which maximizes the heat transport across the outer boundary of the model planet's surface. In order to investigate the impact of the presence of the continents on surface heat flux we have also integrated a model which includes a 50 km

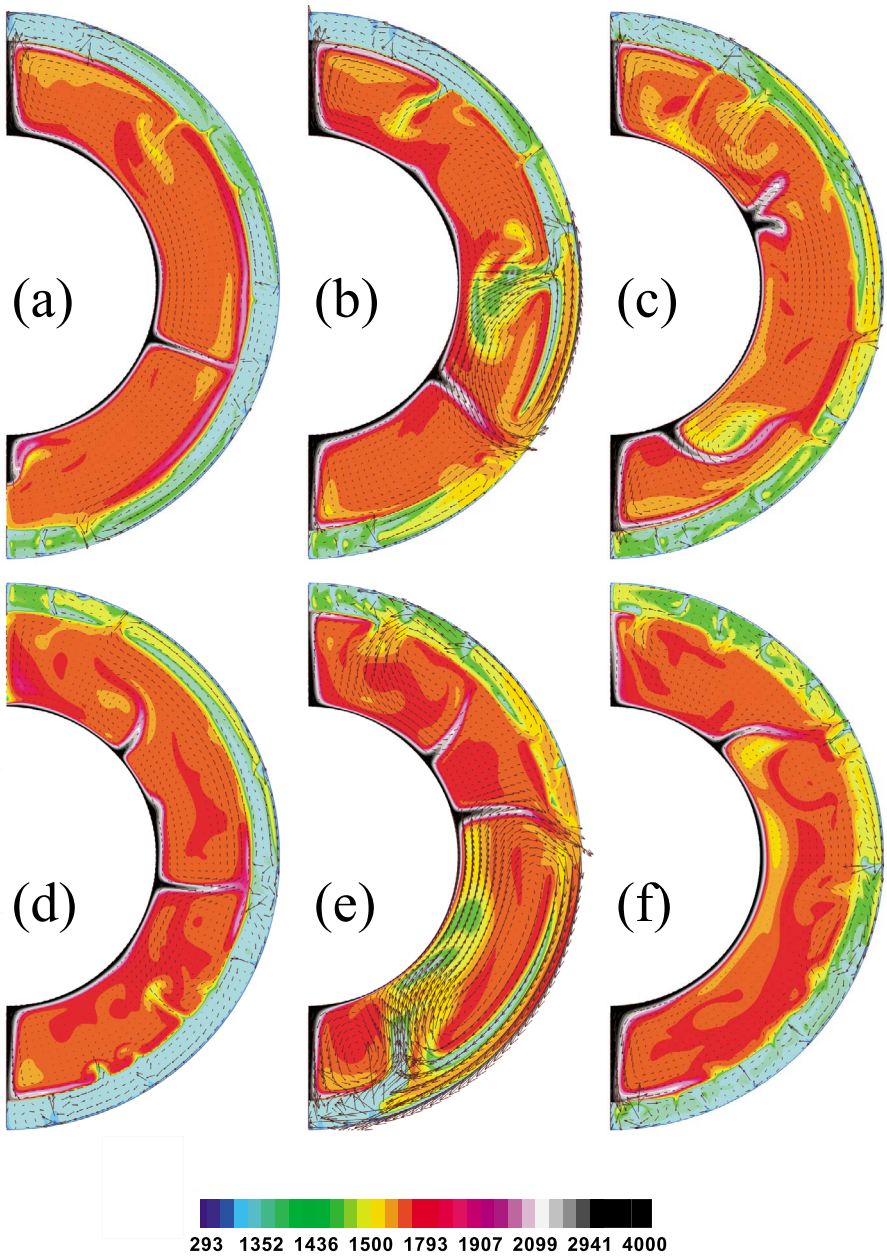

Figure 5. Temperature snapshots of the model C00D00VM3 having CMB temperature of 4000 K at (a) 230 Myr, (b)390 Myr, (c) 500 Myr, (d) 1960 Myr, (e) 2140 Myr, and (f) 2360 Myr, respectively.

thick crust that is simulated by an increase in viscosity by a factor of 10 in this layer compared to the upper layer viscosity in model C00D00VM3 (C00D00VM3-Crust). The results for this model are listed in Table 2 in which it is shown that a 20% reduction in the surface heat flux is characteristic of this model. The model C08D40VM3-Crust with deep mantle phase transition also reveals a reduction in the surface heat flux (note that the reference model C00D00VM3 has higher heat flux than the model C08D40VM3-Crust).

[39] In the next two sequences of models, we explore the influence of the Clapeyron slope of the endothermic phase transition and the viscosity of the mantle on the degree of layering. The magnitude of the Clapeyron slope at the level of the 660 km depth phase transition is clearly a key parameter insofar as the determination of the degree of layering is concerned and it was previously believed that it was best characterized by a numerical value of approximately −2.8 MPa/K. As mentioned in section 1, more recent experimental measurements have suggested that this initial estimate of the Clapeyron slope was excessive. However, under upper mantle conditions, as previously discussed, spinel + stishovite transforms into ilmenite and ilmenite itself transforms into perovskite via a phase transformation which would elevate the effective Clapeyron slope of this combination of phase transformations implying that the more recent high pressure measurements of the spinel →

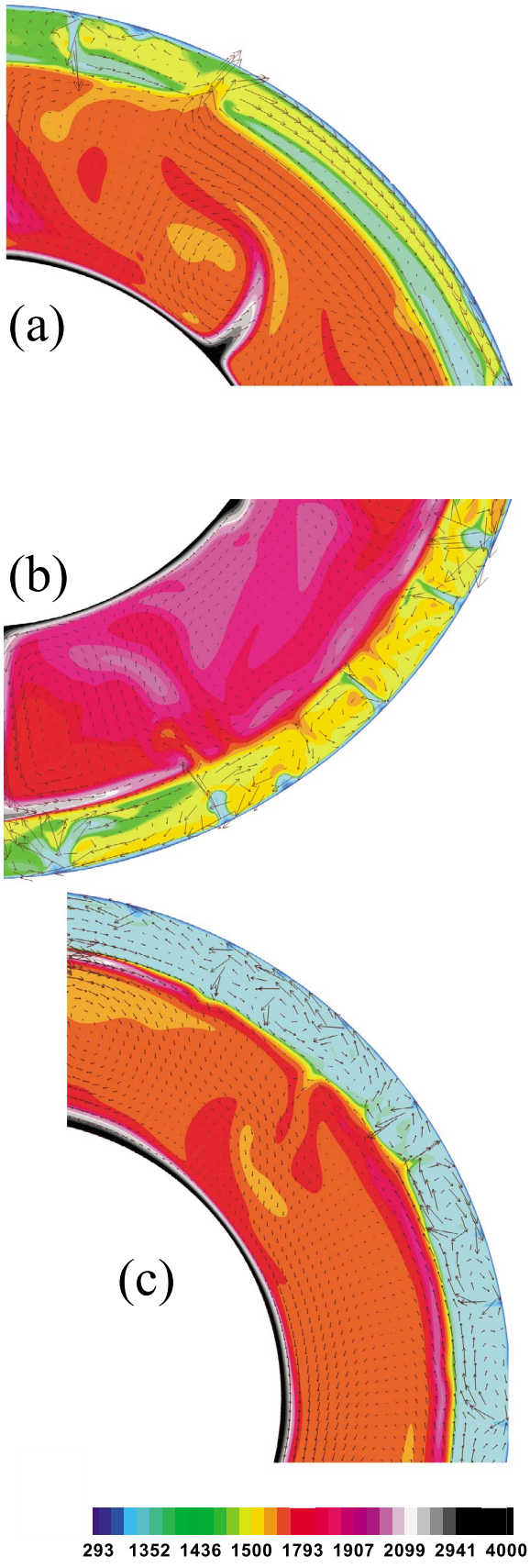

Figure 6. Three temperature close-ups reflecting the coupling between the upper mantle and the lower mantle as described in the text.

perovskite + magnesiowustite transition by *Katsura et al.* [2003] and *Fei et al.* [2004] should not be interpreted as ruling out the plausibility of phase transition induced episodic layering.

[40] In order to study the influence of this effective Clapeyron slope of the 660 km array of phase transformations on the degree of layering, we have computed results for a number of models with different Clapeyron slopes for the endothermic phase transition boundary. The time-averaged radial mass flux time series for these models are shown in Figure 8. Layered convection essentially disappears in models with an effective Clapeyron slope at this boundary of −2.0 MPa/K or less. However, in the models with Clapeyron slope of −2.8 MPa/K, despite the fact that the mixing between the upper mantle and lower mantle is slightly higher, the mass flux minimum in the vicinity of the endothermic transition at 660 km depth persists.

[41] We have devoted the last set of numerical integrations to demonstrating the influence of the mantle viscosity profile on the degree to which the convective circulation is layered. The results are summarized in Table 3. It is well known that the viscosity contrast between the upper mantle and lower mantle alone cannot induce a layered style of convection [e.g., *Peltier*, 1973]; however, in the presence of the endothermic phase transition an increase in viscosity across this boundary may increase the tendency to layered flow. The final set of numerical models span a range of viscosity contrasts of 5, 10, 20, and 50 between the upper and lower mantle while keeping the viscosity in the upper mantle and transition zone fixed to a constant value of 4×10^{20} Pa s. All models have near surface exothermic and endothermic phase transitions and 13 TW of internal heating. Time series for the mass flux across 660 km depth and the time-averaged radial mass flux for these models are displayed in Figure 9. From Figures 9c and 9d, it is clear that the frequency of avalanche events decreases with increasing viscosity contrast between the upper mantle and the lower mantle and that in the model with highest viscosity contrast these events appear to be more diffuse and less intense. It must be noted that, on the basis of the analysis of postglacial rebound data, the factor of 5 increase in viscosity across this horizon is an approximate upper bound.

7. Discussion

[42] The issue of the style of mantle convection has remained a significant focus of interest in the geodynamics and geochemistry communities for decades. As reviewed in section 1, the totality of the constraints that may be brought to bear on this problem, from seismology, isotope geochemistry, and mineral physics as well as from the results delivered by numerical models of the convection process, appear to be most parsimoniously understood by a scenario in which the layering is episodic. Even though a significantly higher-viscosity lower mantle may seem to provide a mechanism for the relative isolation of such a reservoir, finite viscosity contrast alone cannot of itself prevent large-scale mixing across the 660 km depth horizon [*Peltier*, 1973; *van Keken and Ballentine*, 1998]. The early models of *Peltier and Solheim* [1992] and *Solheim and Peltier* [1994a, 1994b] successfully predict this mode of behavior if it is assumed that the penetration inhibiting influence of

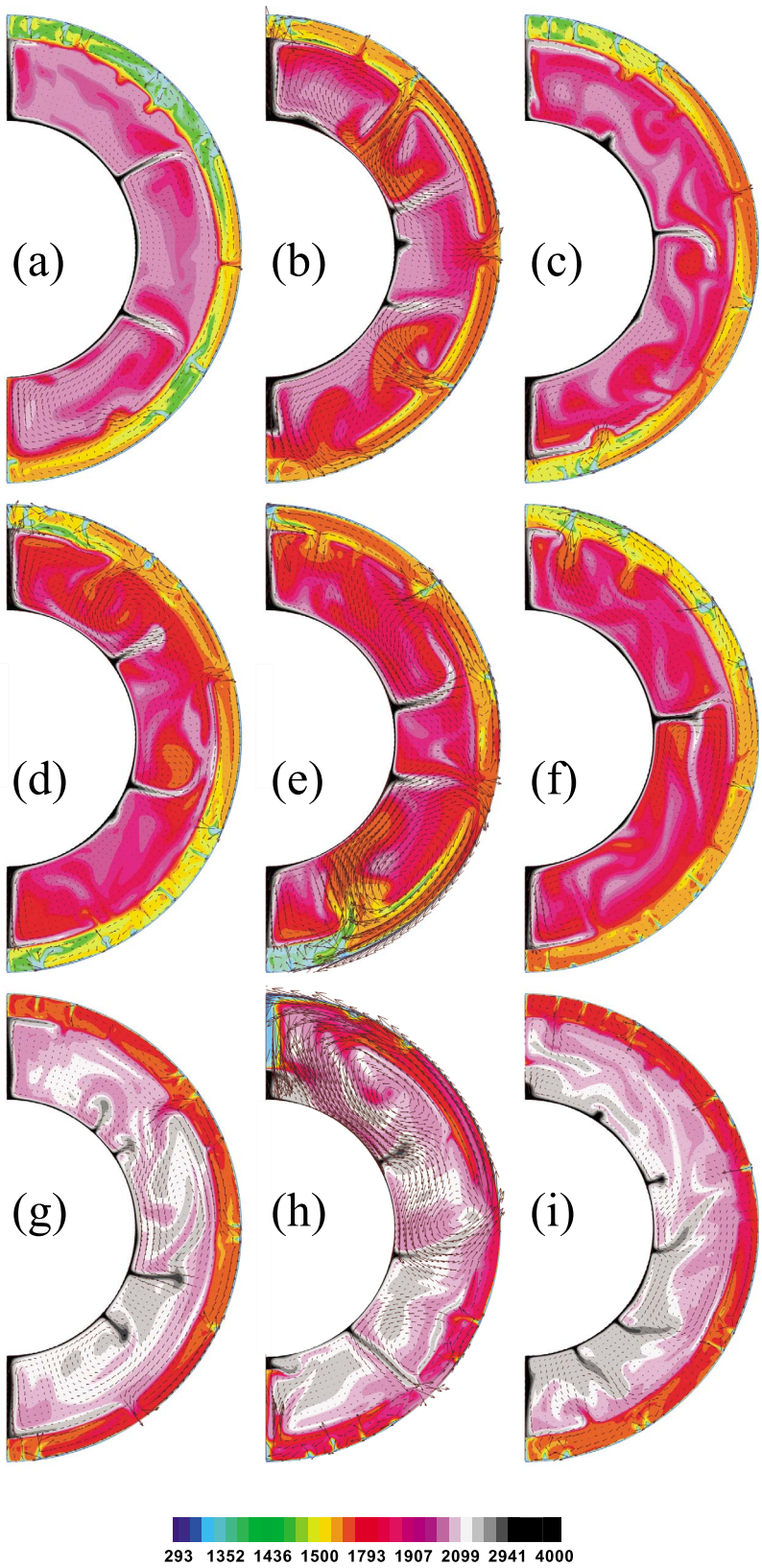

Figure 7. Temperature snapshots of the model C16D80VM3 at (a) 780 Myr, (b) 860 Myr, (c) 1020 Myr; the model C00D00VM3-LS at (d) 320 Myr, (e) 460 Myr, and (f) 560 Myr; the model C16D80VM3-LS at (g) 820 Myr, (h) 970 Myr, and (i) 1100 Myr. The CMB temperature of all models is 4000 K.

Table 2. Time-Averaged (3 Gyr) Mantle Mean Temperature, Surface Heat Flow, Mass Flux Across the Exothermic Phase Boundary at 410 km Depth, Mass Flux Across the Endothermic Phase Boundary at 660 km Depth, and Mass Flux Across the Pv-pPv Phase Boundary at 2700 km Depth, for the Reference Model C00D00VM3, C00D00VM3-Crust, and C08D40VM3-Crust

Model/CMB: 3600 K	T (K)	HF_Surf (TW)	MF_410 (kg/m^2/yr)	MF_660 (kg/m^2/yr)	MF_2700 (kg/m^2/yr)
C00D00VM3	1498	45.4	35.7	28.0	14.6
C00D00VM3-Crust	1817	36.6	21.5	16.8	11.2
C08D40VM3-Crust	1895	39.3	23.5	20.5	15.1

the endothermic phase transitions that occur at the base of the mantle transition zone is sufficiently strong. In the models presented in these earlier papers and in the more detailed models presented herein, this requires that the "effective" Clapeyron slope of the collectivity of these endothermic transitions be sufficiently negative. We have pointed out here that, although the slope of the spinel → perovskite + magnesiowustite transition may be insufficient on its own to satisfy the requirement, when account is taken of the contribution from the ilmenite → perovskite transition that is expected to be active in the vicinity of cold downwellings (Benioff zones), the required degree of inhibition to penetration of the 660 km depth horizon may in fact exist. Additional physical processes also related to the action of these phase transitions, specifically the transformational superplasticity that arises due to the marked reduction in grain size that is an expected consequence of the transformation itself, are expected to further enhance the tendency to layered flow.

[43] In this paper, we have investigated in great detail the nature of the time dependence of the convective mixing process for models in which the dynamical system has been investigated to statistical equilibrium in axisymmetric spherical geometry. Because the interior of the planet cools as the convection process proceeds, such a statistical equilibrium is of course never realized. The database produced by these analyses will nevertheless prove to be extremely useful in the next phase of this new series of analyses of mantle convection in which the new control volume-based model will be deployed in both fully 3-D analyses and in the development of complete thermal histories of Earth evolution. In thermal history mode, the new numerical structure will enable us to considerably refine the recent results of *Butler and Peltier* [2000] that were obtained using the original model of *Solheim and Peltier* [1994a, 1994b]. Our goal will be to more fully explore a possible connection between the episodically layered model of the convective circulation and the so-called "supercontinent cycle" in which continents at Earth's surface are on occasion brought together to form a single "super" continent and then later dispersed. A complete theory will also invoke the thermally insolating nature of the supercontinent itself (as originally envi-

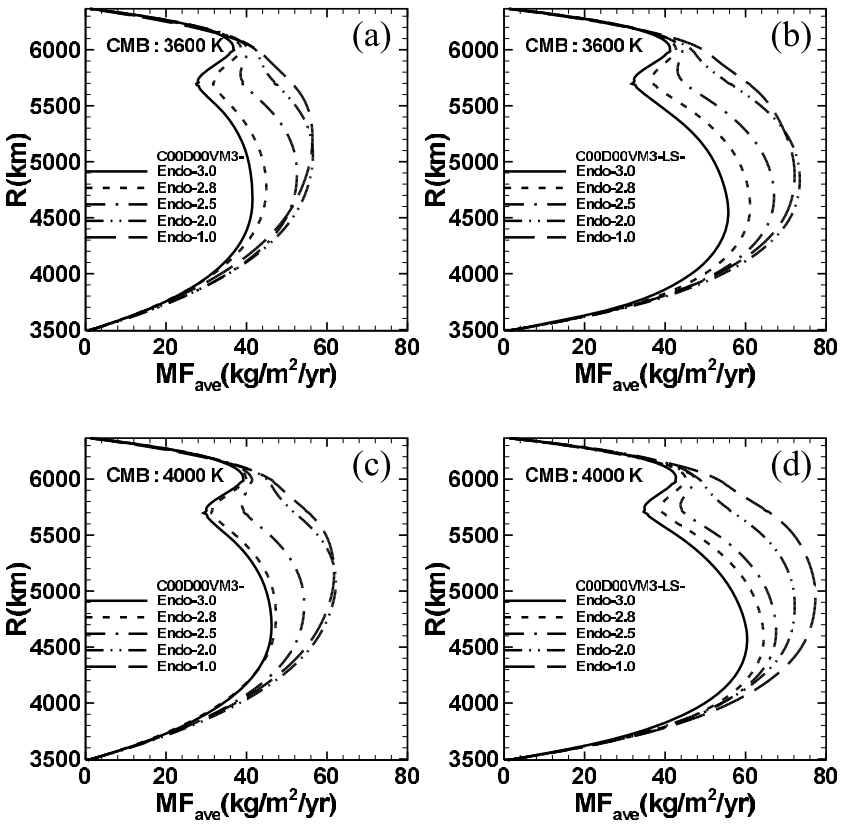

Figure 8. Time-averaged (3 Gyr) radial mass flux for the models with different endothermic Clapeyron slopes with (a) VM3 and (b) VM3-LS viscosity profiles and 3600 K CMB temperatures, and with (c) VM3 and (d) VM3-LS viscosity profiles and 4000 K CMB temperatures.

Table 3. Time-Averaged (10 Gyr) Mantle Mean Temperature, Surface Heat Flow, Mass Flux Across the Exothermic Phase Boundary at 410 km Depth, Mass Flux Across the Endothermic Phase Boundary at 660 km Depth, and Mass Flux Across the Pv-pPv Phase Boundary at 2700 km Depth, for the Models With Different Viscosity Contrasts Between the Upper and Lower Mantle With CMB Temperatures 3600 K and 4000 K

Model	T (K)	HF_Surf (TW)	MF_410 (kg/m^2/yr)	MF_660 (kg/m^2/yr)	MF_2700 (kg/m^2/yr)
		CMB: 3600 K			
C00D00VM3-Step-05	1688	58.7	48.4	41.1	33.5
C00D00VM3-Step-10	1588	53.7	42.6	35.8	23.8
C00D00VM3-Step-20	1515	48.7	35.8	26.8	16.2
C00D00VM3-Step-50	1395	43.1	30.6	21.4	10.4
		CMB: 4000 K			
C00D00VM3-Step-05	1807	65.7	51.7	44.6	35.8
C00D00VM3-Step-10	1709	60.5	44.7	35.3	25.2
C00D00VM3-Step-20	1602	54.3	38.3	29.4	16.8
C00D00VM3-Step-50	1464	46.9	30.8	20.0	10.2

sioned by e.g., *Busse* [1978]) in order to focus the required upwelling beneath the supercontinent that is required to drive the rifting phase of the cycle. In the work of *Peltier et al.* [1997], it was first suggested that this cycle was intimately connected to the avalanche process that is characteristic of the episodically layered convection model. During a typical avalanche all continental fragments within a significant angular displacement from the surface stag-

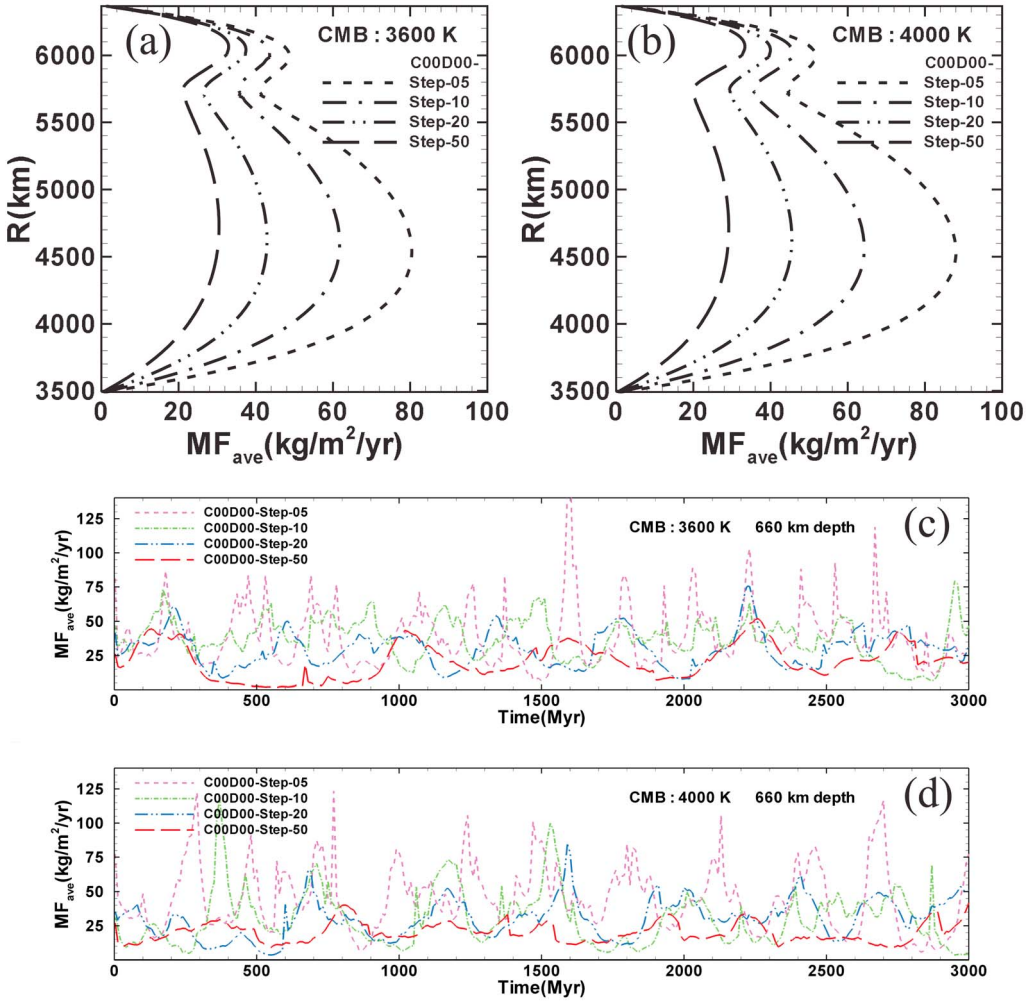

Figure 9. (a) Time-averaged (3 Gyr) radial mass flux for the models with step viscosity profiles of contrast 5, 10, 20, and 50 between the upper and lower mantle for the models with CMB temperatures at (a) 3600 K and (b) 4000 K. Similarly, time series of the mantle absolute mass flux across the 660 km depth phase transition boundaries for the models with CMB temperatures at (c) 3600 K and (d) 4000 K.

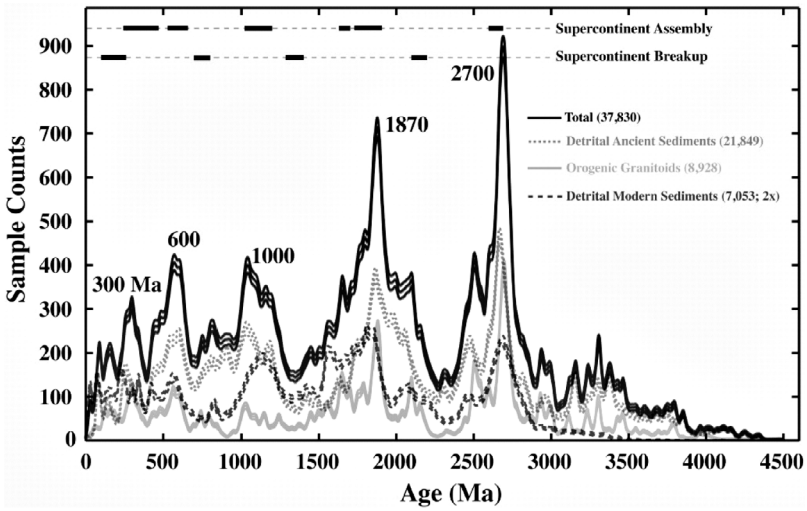

Figure 10. U/Pb zircon age distribution in orogenic granitoids and two types of detrital zircon data sets for the past 4.5 Gyr [*Condie et al.*, 2009b]. Distribution peaks are labeled with time estimates in Myr. The multiple lines in each spectrum represent error bounds of one standard deviation. The detrital modern sediment database is multiplied by 2 for clarity. Numbers of zircon sample ages in each data set are indicated in the legend. The supercontinent assembly and breakup periods are indicated at top (reproduced from *Condie and Aster* [2009c]).

nation point that forms directly above the region of downwelling across the 660 km horizon are drawn toward the stagnation point where they coalesce to form a supercontinent. *Peltier et al.* [1997] suggested that there existed strong observational support for this model in the early data of *Dearnley* [1965] who produced a histogram of the number of surface samples of igneous rocks of a given age as a function of their age. It had been known for some time that this histogram was characterized by the existence of several well-defined peaks separated by a time scale of order 300–500 Myr. Since the episodically layered convection model of *Peltier and Solheim* [1992] predicted precisely this time scale for the separation between successive avalanches, this was construed as strong evidence in favor of the hypothesis.

[44] This idea of a connection between the phase transition modulated mixing scenario for the mantle convection process and the supercontinent cycle was later supported further by the more detailed analysis of the episodicity of granite production by *Condie* [1998] and very recently further analyzed by *Hawkesworth et al.* [2009]. It was argued that the spatially discontinuous and temporally episodic intrusion of silica-rich magma into the crust provides a "mosaic" of ages for granites in a given region [*Condie*, 1998; *Kemp et al.*, 2006]. Caution is clearly required, however, because of the unknown impact of sampling strategy. In particular, it was pointed out that the striking peaks in the histogram based on rocks for the Canadian and Baltic Shields of ages 2.7 and 1.9 billion years could simply be a consequence of the fact that these shields have been extensively sampled.

[45] Recently published new analyses of the age histogram based exclusively upon Zircon dating has served to further support the original interpretation of *Peltier et al.* [1997] and to significantly improve the quality of the observations compared to those of *Dearnley* [1965] on which it was originally based. Because individual zircons are both ubiquitous in the crust and are able to survive processes of erosion, transport, and even high-grade metamorphism, they provide exquisite records of tectonophysical processes. Because this mineral contains trace elements of uranium and thorium, samples may be dated by determining the U/Pb and Th/Pb isotopic ratios. The recently published age histogram by *Condie and Aster* [2009c], which is reproduced here as Figure 10, has a number of important features. The first and dominant peak in the histogram at 2700 Myr is followed by a second equally prominent but somewhat weaker peak of 1870 Myr age. These are essentially the same ages as the two earliest peaks in the Dearnley histogram. As time proceeds, however, and contrary to the Dearnley results, the amplitude of the individual peaks in the histogram decreases and the spacing between them also decreases indicating, according to the interpretation of *Peltier et al.* [1997], that the frequency of the avalanches is increasing [*Condie*, 1998; *Korenaga*, 2006; *Condie et al.*, 2009a, 2009b]. On the basis of neodymium and hafnium isotopic data, *Condie and Aster* [2009c] have argued in favor of increased preservation of the juvenile continental crust rather than increasing crustal production to account for the diminishing amplitude of the individual peaks in the spectrum. In our view this remains an open issue.

[46] Although it will require detailed further analyses of the thermal history of the planet so as to extend the results of *Butler and Peltier* [2000, 2002] in order to make close contact with these recent results of Condie and others, an initial analysis based on results from the current model is worthwhile. To this end, we show in Figure 11 the cooling history result from the model C00D00VM3 (CMB temperature held fixed at 4000 K) in which the initial mean temperature is ~280 K higher. The initial temperature for this model was obtained from another model with the Pv-pPv transition included which increases the mantle mean temperature. This is clearly an "out of statistical equilibrium"

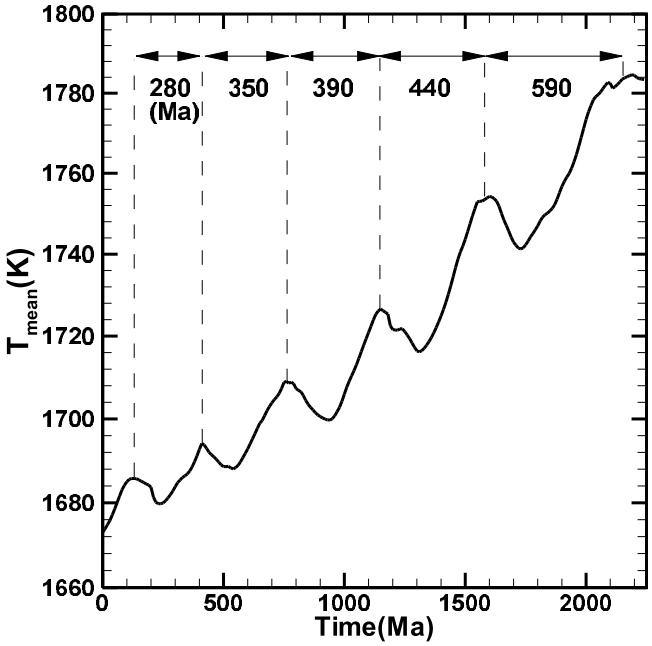

Figure 11. Time series of the mean mantle temperature for the model C00D00VM3 started with a higher mantle temperature. The period of avalanche cycles decreases with time as the Earth is cooling.

analysis. Over the 2000 Myr interval for which the integration was continued, the mantle cools by approximately 100 K, and the avalanche frequency clearly increases in agreement with the results of Condie et al. discussed in the previous paragraphs of this section. The full thermal history analyses required to more fully explore the ability of the model to reconcile these observations will be reported elsewhere.

8. Conclusions

[47] In the main body of this paper, we have explored the implications of the existence of the recently discovered post-perovskite transition insofar as the episodically layered model of the mantle convective circulation is concerned. The most recent mantle parameters based on mineral physics models have been employed. The identification of this transition by *Murakami et al.* [2004] provides the best available explanation of the properties of the D'' layer, as these have been inferred on seismological grounds. Aside from providing a natural explanation for the seismic anisotropy of this region, the existence of this transition would also appear to eliminate the necessity of invoking partial melting for the explanation of the existence of ultra low velocity zones (ULVZ) within D''. It also provides the most natural explanation of the discontinuity in S-velocity that occurs at the top of D'' itself.

[48] This new solid-solid phase transition that appears to be stable under deep mantle conditions in regions that are sufficiently cold could also significantly impact mantle dynamics and thus the cooling of the core and the thermal history of the planet. This issue has provided the motivation for the present work in which we have explored the impact of this new phase transition on the dynamics of thermal plumes that originate through the instability of the D'' layer itself and of the extent to which the expected episodically layered state of convection may be affected. In this regard, we have investigated the extent to which the increased vigor of mantle plumes originating in boundary layer instability of D'' may decrease the ability of the endothermic transition at 660 km depth to enforce an episodically layered style of mantle circulation. In four sets of numerical models using a control volume formulation, we have systematically investigated the influence of this Pv-pPv phase transition by analyzing the impact of a wide range of density contrasts and Clapeyron slopes for the new phase transition that appear to cover the experimentally allowed variations.

[49] Some previous thermal and thermochemical convection models have also suggested that the dynamical effect of the Pv-pPv phase transition is small and that the mantle temperature is slightly higher in the presence of this deep mantle phase transition than in its absence [*Tackley et al.*, 2007]. However, our numerical models reveal that the presence of this new exothermic phase transition that appears to define the D'' layer adjacent to the CMB enhances the degree of instability of the lower thermal boundary layer to an extent that is expected to depend significantly on the temperature dependence of the rheology of mantle material [*Yuen and Peltier*, 1980]. This extra forcing mechanism enhances the vigor of mantle plumes and thus the rate of core cooling. This layer is almost certainly the origin of mantle superplumes.

[50] The extent to which the convective circulation is layered is enhanced by increasing the Rayleigh number [*Solheim and Peltier*, 1994a] and the presence of the deep mantle exothermic phase transition enhances the circulation which could be considered analogous to the expected characteristics of convection at higher Rayleigh number. However, as we have shown, it also enhances the mass transfer between the upper mantle and the lower mantle, which also impacts the degree of mantle layering. Our numerical models reveal that, although the presence of the new phase transition enhances the vigor of the convective circulation and generally weakens mantle layering, the episodically layered pattern of convection persists even in the models having double the Clapeyron slope for the Pv-pPv transition than that constrained experimentally. The inclusion of a low-viscosity layer above the core mantle boundary causes a further increase in the vigor of the mixing processes; however, even in this case the net effect of the deep mantle low-viscosity layer and the deep mantle exothermic phase transition do not eliminate the episodically layered character of the mixing process. It is through this episodicity that we continue to search for a detailed explanation of the supercontinent cycle.

[51] **Acknowledgments.** M.H.S. thanks Jafar Arkani-Hamed for financial support early in this project. The computations on which the paper is based were performed on the SciNet facility for high-performance computation, which is a component of the Compute Canada platform. Additional support was provided by NSERC discovery grant A9627 to W.R.P.

References

Allegre, C. J., A. Hofmann, and K. O'Nions (1996), The argon constraints on mantle structure, *Geophys. Res. Lett.*, *23*(24), 3555–3557, doi:10.1029/96GL03373.

Anderson, D. L. (1998), The helium paradoxes, *Proc. Natl. Acad. Sci. U. S. A.*, *95*, 4822–4827.
Boehler, R. (1992), Melting of the Fe-FeO and the Fe-FeS systems at high pressure: Constraints on core temperatures, *Earth Planet. Sci. Lett.*, *111*, 217–227.
Brandt, A. (1982), Guide to multigrid development, *Lect. Notes Math.*, *960*, 220–312.
Bullen, K. E. (1950), An Earth model based on compressibility-pressure hypothesis, *Mon. Not. R. Astron. Soc. Geophys. Suppl.*, *6*, 50–59.
Busse, F. H. (1978), A model of time-periodic mantle flow, *Geophys. J. R. Astron. Soc.*, *52*, 1–12.
Butler, S. L., and W. R. Peltier (2000), On scaling relations in time-dependent mantle convection and the heat transfer constraint on layering, *J. Geophys. Res.*, *105*(B2), 3175–3208, doi:10.1029/1999JB900377.
Butler, S. L., and W. R. Peltier (2002), Thermal evolution of Earth: Models with time-dependent layering of mantle convection which satisfy the Urey ratio constraint, *J. Geophys. Res.*, *107*(B6), 2109, doi:10.1029/2000JB000018.
Cadek, O., and L. Fleitout (2006), Effect of lateral viscosity variations in the core–mantle boundary region on predictions of the long wavelength geoid, *Stud. Geophys. Geod.*, *50*, 217–232.
Christensen, U. R., and D. A. Yuen (1984), The interaction of a subducting lithospheric slab with a chemical or phase boundary, *J. Geophys. Res.*, *89*(B6), 4389–4402, doi:10.1029/JB089iB06p04389.
Christensen, U. R., and D. A. Yuen (1985), Layered convection induced by phase transitions, *J. Geophys. Res.*, *90*(B12), 10,291–10,300, doi:10.1029/JB090iB12p10291.
Cizkova, H., O. Cadek, C. Matyska, and D. A. Yuen (2010), Implications of post-perovskite transport properties for core-mantle dynamics, *Phys. Earth Planet. Inter.*, *180*, 235–243, doi:10.1016/j.pepi.2009.08.008.
Condie, K. C. (1998), Episodic continental growth and supercontinents: A mantle avalanche connection?, *Earth Planet. Sci. Lett.*, *163*, 97–108.
Condie, K. C., E. Belousova, W. L. Griffin, and K. N. Sircombe (2009a), Granitoid events in space and time: Constraints from igneous and detrital zircon age spectra, *Gondwana Res.*, *15*(3–4), 228–242.
Condie, K., C. O'Neill, and R. Aster (2009b), Evidence and implications for a widespread magmatic shutdown for 250 My on Earth, *Earth Planet. Sci. Lett.*, *282*, 294–298.
Condie, K. C., and R. C. Aster (2009c), Zircon age episodicity and growth of continental crust, *Eos Trans. AGU*, *90*(41), 364, doi:10.1029/2009EO410003.
Creager, K. C., and T. H. Jordan (1986), Slab penetration into the lower mantle beneath the Mariana and other island arcs of the northwest Pacific, *J. Geophys. Res.*, *91*(B3), 3573–3580, doi:10.1029/JB091iB03p03573.
Dahm, C. G. (1934), A study of Dilatational wave velocity in the Earth as a function of depth, based on a comparison of the *P*, *P″* and *PcP* phases, Ph.D. dissertation, St. Louis Univ., St. Louis, Mo.
Davies, G. F., and M. A. Richards (1992), Mantle convection, *J. Geol.*, *100*, 151–206.
Davies, G. F. (1999), Geophysically constrained mantle mass flows and the ^{40}Ar budget: A degassed lower mantle?, *Earth Planet. Sci. Lett.*, *166*, 149–162.
Deal, M. M., and G. Nolet (1999), Slab temperature and thickness from seismic tomography 2. Izu-Bonin, Japan, and Kuril subduction zones, *J. Geol. Res.*, *104*(12), 28,803–28,812.
Dearnley, R. (1965), Orogenic fold belts and continental drift, *Nature*, *206*, 1083–1087.
Fei, Y. (1995), *Thermal expansion in Mineral Physics and Crystallography: A Handbook of Physical Constants*, vol. 2, edited by T. J. Ahrens, pp. 64–97, AGU, Washington, D. C.
Fei, Y., J. Van Orman, J. Li, W. van Westrenen, C. Sanloup, W. Minarik, K. Hirose, T. Komabayashi, M. Walter, and K. Funakoshi (2004), Experimentally determined post-spinel transformation boundary in Mg_2SiO_4 using MgO as an internal pressure standard and its geophysical implications, *J. Geophys. Res.*, *109*, B02305, doi:10.1029/2003JB002562.
Fiquet, G., A. Dewaele, D. Andrault, M. Kunz, and T. Le Bihan (2000), Thermoelastic properties and crystal structure of $MgSiO_3$ perovskite at lower mantle pressure and temperature conditions, *Geophys. Res. Lett.*, *27*(1), 21–24, doi:10.1029/1999GL008397.
Fiquet, G. (2001), Mineral phases of the Earth's mantle, *Z. Krist.*, *216*, 248–271.
Forte, A. M., W. R. Peltier, A. M. Dziewonski, and R. L. Woodward (1993), Dynamic Surface Topography: A new interpretation based on mantle flow models derived from seismic tomography, *Geophys. Res. Lett.*, *20*(3), 225–228, doi:10.1029/93GL00249.
Fukao, Y., M. Obayashi, H. Inoue, and M. Nenbai (1992), Subducting Slabs Stagnant in the Transition Zone, *J. Geophys. Res.*, *97*(B4), 4809–4822, doi:10.1029/91JB02749.
Garnero, E. J., and T. Lay (2003), *D″* shear velocity heterogeneity, anisotropy and discontinuity structure beneath the Caribbean and Central America, *Phys. Earth Planet. Inter.*, *140*(1–3), 219–242.
Grand, S. P. (2002), Mantle shear wave tomography and the fate of subducted slabs, *Philos. Trans. R. Soc. Ser. A*, *360*(1800), 2475–2491.
Hawkesworth, C., P. Cawood, T. Kemp, C. Storey, and B. Dhuime (2009), A matter of preservation, *Science*, *323*, 49–50.
Helmberger, D. V., T. Lay, S. Ni, and M. Gurnis (2005), Deep mantle structure and the post-perovskite phase transition, *Proc. Natl. Acad. Sci. U. S. A.*, *102*, 17,257–17,263, doi:10.10732/pnas.05023504102.
Hernlund, J. W., C. Thomas, and P. J. Tackley (2005), A doubling of the post-perovskite phase boundary and structure of the Earth's lowermost mantle, *Nature*, *434*, 882–886.
Hofmeister, A. M. (1999), Mantle values of thermal conductivity and the geotherm from phonon lifetimes, *Science*, *283*, 1699–1706.
Hong, D., J. Zhang, T. Wang, S. Wang, and X. Xie (2004), Continental crustal growth and the supercontinental cycle: Evidence from the Central Asian Orogenic Belt, *J. Asian Earth Sci.*, *23*, 799–813.
Hunt, S. A., D. J. Weidner, L. Li, L. Wang, N. P. Walte, J. P. Brodholt, and D. P. Dobson (2009), Weakening of calcium iridate during its transformation from perovskite to post-perovskite, *Nat. Geosci.*, *2*, 794–797.
Ito, E., and E. Takahashi (1989), Post-spinel transformations in the system Mg_2SiO_4–Fe_2SiO_4 and some geophysical implications, *J. Geophys. Res.*, *94*(B8), 10,637–10,646, doi:10.1029/JB094iB08p10637.
Ito, E., and H. Sato (1991), Aseismicity in the lower mantle by superplasticity of the descending slab, *Nature*, *351*, 140–141.
Jordan, T. H., P. Puster, G. A. Glazmaier, and P. J. Tackley (1993), Comparisons between seismic earth structures and mantle flow models based on radial correlation functions, *Science*, *261*, 1427–1431.
Karato, S.-I., S. Zhang, and H.-R. Wenk (1995), Superplasticity in Earth's lower mantle: Evidence from seismic anisotropy and rock physics, *Science*, *270*, 458–461.
Kato, T., E. Ohtani, H. Morishima, D. Yamazaki, A. Suzuki, M. Suto, and T. Kubo (1995), In situ X ray observation of high-pressure phase transitions of $MgSiO_3$ and thermal expansion of $MgSiO_3$ perovskite at 25 GPa by double-stage multi-anvil system, *J. Geophys. Res.*, *100*(B10), 20,475–20,481, doi:10.1029/95JB01688.
Katsura, T., H. Yamada, T. Shinmei, A. Kubo, S. Onoa, M. Kanzaki, A. Yoneda, and M. J. Walter (2003), Post-spinel transition in Mg_2SiO_4 determined by high P-T in situ X-ray diffractometry, *Phys. Earth Planet. Inter.*, *136*(1–2), 11–24.
Kemp, A. I. S., C. J. Hawkesworth, B. A. Paterson, and P. D. Kinny (2006), Episodic growth of the Gondwana supercontinent from hafnium and oxygen isotopes in zircon, *Nature*, *439*, 581–583.
Kennett, B. L. N., S. Widiyantoro, and R. D. van der Hilst (1998), Joint seismic tomography for bulk-sound and shear waves peed in the Earth's mantle, *J. Geophys. Res.*, *103*(B6), 12,469–12,493, doi:10.1029/98JB00150.
King, S. D. (1995), Models of mantle viscosity, in *Mineral Physics and Crystallography: A Handbook of Physical Constants*, *AGU Ref. Shelf*, vol. 2, edited by T. J. Ahrens, pp. 227–236, AGU, Washington, D. C.
Kirby, S. H. (1983), Rheology of the lithosphere, *Rev. Geophys. Space Phys.*, *21*, 1458–1487.
Korenaga, J. (2006), Archean geodynamics and the thermal evolution of Earth, in *Archean Dynamics and Environments*, *Geophys. Monogr. Ser.*, vol. 164, edited by K. Benn, J. C. Mareschal, and K. C. Condie, pp. 7–32, AGU, Washington D. C.
Krylov, A., B. A. Mamyrin, L. A. Khabarin, T. I. Mazina, and Y. I. Silin (1974), Helium isotopes in ocean floor bedrock, *Geokhim.*, *8*, 1220–1225.
Kumar, M. (2000), Equation of state and bulk modulus under the effect of high pressure-high temperature, *Phys. Chem. Miner.*, *27*, 650–655.
Lay, T. (2005), The deep mantle thermo-chemical boundary layer: The putative mantle plume source, in *Plates, Plumes, and Paradigms*, edited by G. R. Foulger et al., *Spec. Pap. Geol. Soc. Am.*, *388*, 193–205.
Lay, T., E. J. Garnero, and Q. Williams (2004), Partial melting in a thermo-chemical boundary layer at the base of the mantle, *Phys. Earth Planet. Inter.*, *146*, 441–467.
Lay, T., and D. V. Helmberger (1983), A shear velocity discontinuity in the lower mantle, *Geophys. Res. Lett.*, *10*(1), 63–66, doi:10.1029/GL010i001p00063.
Lupton, J. E., and H. Craig (1975), Excess ^{3}He in oceanic basalts: Evidence for terrestrial primordial helium, *Earth Planet. Sci. Lett.*, *26*, 133–139.
Mao, W. L., G. Shen, V. B. Prakapenka, Y. Meng, A. J. Campbell, D. L. Heinz, J. Shu, R. J. Hemley, and H. K. Mao (2004), Ferromagnesian post-perovskite silicates in the *D″* layer of the Earth, *Proc. Natl. Acad. Sci. U. S. A.*, *101*(45), 15,867–15,869.
Mao, W. L., H.-K. Mao, W. Sturhahn, J. Zhao, V. B. Prakapenka, Y. Meng, J. Shu, Y. Fei, and R. J. Hemley (2006), Iron-rich post-perovskite and the origin of ultralow-velocity zones, *Science*, *312*, 564–565.

Matsuda, J., M. Sudo, M. Ozima, K. Ito, O. Ohtaka, and E. Ito (1993), Noble gas partitioning between metal and silicate under high pressure, *Science*, *259*, 788–790.

Matyska, C., and D. A. Yuen (2005), The importance of radiative heat transfer on superplumes in the lower mantle with the new post-perovskite phase change, *Earth Planet. Sci. Lett.*, *234*(1–2), 71–81.

Meade, C., and P. G. Silver (1995), Laboratory and seismological observation of lower mantle isotropy, *Geophys. Res. Lett.*, *22*(10), 1293–1296, doi:10.1029/95GL01091.

Monnereau, M., and D. A. Yuen (2007), Topology of the post-perovskite phase transition and mantle dynamics, *Proc. Natl. Acad. Sci. U. S. A.*, *104*(22), 9156–9161.

Monnereau, M., and D. A. Yuen (2010), Seismic imaging of the D″ and constraints on the core heat flux, *Phys. Earth Planet. Inter.*, doi:10.1016/j.pepi.2009.1012.1005.

Murakami, M., K. Hirose, K. Kawamura, N. Sata, and Y. Ohishi (2004), Post-perovskite phase transition in $MgSiO_3$, *Science*, *304*, 855–858.

Nakagawa, T., and P. J. Tackley (2004), Effects of a perovskite-post-perovskite phase change near core-mantle boundary in compressible mantle convection, *Geophys. Res. Lett.*, *31*, L16611, doi:10.1029/2004GL020648.

Oganov, A. R., and S. Ono (2004), Theoretical and experimental evidence for post-perovskite phase of Mg SiO_3 in Earth's *D″* layer, *Nature*, *430*, 445–448.

Ono, S., Y. Ohishi, and K. Mibe (2004), Phase transition of Ca-perovskite and stability of Al-bearing Mg-perovskite in the lower mantle, *Am. Mineral.*, *89*(10), 1480–1485.

Pari, G., and W. R. Peltier (1995), The heat flow constraint on mantle tomography-based convection models: Toward a geodynamically self-consistent inference of mantle viscosity, *J. Geophys. Res.*, *100*(B7), 12,731–12,751, doi:10.1029/95JB01078.

Patankar, S. V. (1980), *Numerical Heat Transfer and Fluid Flow*, Hemisphere, Washington, D. C.

Peltier, W. R. (1973), Penetrative convection in the planetary mantle, *Geophys. Astrophys. Fluid Dyn.*, *5*(1), 47–88.

Peltier, W. R. (1980), Mantle convection and viscosity, in *Physics of the Earth's Interior, Proceedings of the Enrico Fermi Summer School in Physics*, edited by A. Dziewonski and E. Boschi, pp. 362–431, North Holland Publ. Co., Amsterdam.

Peltier, W. R. (1996), Phase-transition modulated mixing in the mantle of the earth, *Philos. Trans. R. Soc. Ser. A*, *354*, 1425–1447.

Peltier, W. R. (1998a), The inverse problem for mantle viscosity, *Inverse Problems*, *14*, 441–478.

Peltier, W. R. (1998b), Global glacial isostasy and relative sea level: Implications for solid earth geophysics and climate system dynamics, *Geo Res. Forum*, *3–4*, 17–54.

Peltier, W. R., and R. Drummond (2010), Deepest mantle viscosity: Constraints from Earth rotation anomalies, *Geophys. Res. Lett.*, *37*, L12304, doi:10.1029/2010GL043219.

Peltier, W. R., and X. Jiang (1996), Glacial isostatic adjustment and earth rotation: Refined constrains on the viscosity of the deepest mantle, *J. Geophys. Res.*, *101*(B2), 3269–3290, doi:10.1029/95JB01963.

Peltier, W. R., and X. Jiang (1997), Mantle viscosity, glacial isostatic adjustment and the Eustatic level of the sea, *Surv. Geophys.*, *18*(2–3), 239–277.

Peltier, W. R., S. Butler, and L. P. Solheim (1997), The influence of phase transformation on mantle mixing and plate tectonics, in *Earth's Deep Interior*, edited by D. J. Crossley, pp. 405–430, Gordon and Breach, Amsterdam.

Peltier, W. R., and L. P. Solheim (1992), Mantle phase transitions and layered chaotic convection, *Geophys. Res. Lett.*, *19*(3), 321–324, doi:10.1029/91GL02951.

Peltier, W. R. (2007), Mantle dynamics and the *D″* layer: Impacts of the post-perovskite phase, in *Post-Perovskite: The Last Mantle Phase Transition*, *Geophys. Monogr. Ser.*, vol. 174, edited by K. Hirose et al., pp. 217–227, AGU, Washington, D. C.

Poirier, J. P. (1985), *Creep of Crystals*, 264 pp., Cambridge Univ. Press, Cambridge.

Ranalli, G. (1987), *Rheology of the Earth: Deformation and Flow Processes in Geophysics and Geodynamics*, 366 pp., Allen and Unwin, Boston.

Ranalli, G. (1991), The microphysical approach to mantle rheology, in *Glacial Isostasy, Sea-Level, and Mantle Rheology*, edited by R. Sabadini, K. Lambeck, and E. Boschi, pp. 343–378, Kluwer Acad., London.

Saxena, S. K., L. S. Dubrovinsky, P. Lazor, Y. Cerenius, P. Häggkvist, M. Hanfland, and J. Hu (1996), Stability of perovskite ($MgSiO_3$) in the Earth's mantle, *Science*, *274*, 1357–1359.

Schmeling, H., G. Marquart, and T. Ruedas (2003), Pressure and temperature-dependent thermal expansivity and the effect on mantle convection and surface observables, *Geophys. J. Int.*, *154*(1), 224–229.

Schmid, C., S. Goes, S. van der Lee, and D. Giardini (2002), Fate of the Cenozoic Farallon slab from a comparison of kinematic thermal modeling with tomographic images, *Earth Planet. Sci. Lett.*, *204*(1–2), 17–32.

Schubert, G., G. Masters, P. Olson, and P. J. Tackley (2004), Superplumes or plume clusters? *Phys. Earth Planet. Inter.*, *146*, 147–162.

Serghiou, G., A. Zerr, and R. Boehler (1998), (Mg, Fe)SiO_3-perovskite stability under lower mantle conditions, *Science*, *280*, 2093–2095.

Shim, S. H., T. S. Duffy, and G. Y. Shen (2001), Stability and structure of $MgSiO_3$ perovskite to 2300-kilometer depth in Earth's mantle, *Science*, *293*, 2437–2440.

Sidorin, I., M. Gurnis, and D. V. Helmberger (1999), Evidence for ubiquitous seismic discontinuity at the base of mantle, *Science*, *286*, 1326–1331.

Silver, P. G., S. Kaneshima, and C. Meade (1993), Why is the lower manfie so isotropic?, *Eos Trans. AGU*, *74*(16), Spring Meet. Suppl., S313.

Solheim, L. P., and W. R. Peltier (1993), Mantle phase transitions and layered convection, *Can. J. Earth Sci.*, *30*(5), 881–892.

Solheim, L. P., and W. R. Peltier (1994a), Avalanche effects in phase transition modulated thermal convection: A model of Earth's mantle, *J. Geophys. Res.*, *99*(B4), 6997–7018, doi:10.1029/93JB02168.

Solheim, L. P., and W. R. Peltier (1994b), Phase boundary deflections at 660 km depth and episodically layered isochemical convection in the mantle, *J. Geophys. Res.*, *99*(B8), 15,861–15,875, doi:10.1029/94JB00730.

Stein, M., and A. W. Hofmann (1994), Mantle plumes and episodic crustal growth, *Nature*, *372*, 63–68.

Su, W., and A. M. Dziewonski (1997), Simultaneous inversion for 3-D variations in shear and bulk velocity in the mantle, *Phys. Earth Planet. Inter.*, *100*, 135–156.

Tackley, P. J., T. Nakagawa, and J. W. Hernlund (2007), Influence of the post-perovskite transition on thermal and thermo-chemical mantle convection, in *The Last Mantle Phase Transition*, edited by K. Hirose et al., pp. 229–248, AGU, Washington, D. C.

Turekian, K. K. (1959), The terrestrial economy of helium and argon, *Geochim. Cosmochim. Acta*, *17*, 37–43.

van den Berg, A. P., D. A. Yuen, and J. R. Allwardt (2002), Non-linear effects from variable thermal conductivity and mantle internal heating: Implications for massive melting and secular cooling of the mantle, *Phys. Earth Planet. Inter.*, *129*(3–4), 359–375.

van der Hilst, R., R. Engdahl, W. Spakman, and G. Nolet (1991), Tomographic imaging of subducted lithosphere below Northwest Pacific Island Arcs, *Nature*, *353*, 37–43.

van der Hilst, R. D., M. V. de Hoop, P. Wang, S. H. Shim, P. Ma, and L. Tenorio (2007), Seismostratigraphy and thermal structure of Earth's core-mantle boundary region, *Science*, *315*, 1813, doi:10.1126/science.1137867.

van Keken, P. E., and C. J. Ballentine (1998), Whole-mantle versus layered mantle convection and the role of a high-viscosity lower mantle in terrestrial volatile evolution, *Earth Planet. Sci. Lett.*, *156*, 19–32.

Yuen, D. A., and W. R. Peltier (1980), Mantle plumes and the thermal stability of the *D″* layer, *Geophys. Res. Lett.*, *7*(9), 625–628, doi:10.1029/GL007i009p00625.

Yuen, D. A., C. Matyska, O. Cadek, and M. Kameyama (2007), The dynamical influences from physical properties in the lower mantle and post-perovskite phase transition, in *The Last Mantle Phase Transition*, edited by K. Hirose et al., pp. 249–270, AGU, Washington, D. C.

Zhao, D. (2004), Global tomographic images of mantle plumes and subducting slabs: Insight into deep Earth dynamics, *Phys. Earth Planet. Inter.*, *146*, 3–34.

W. R. Peltier and M. H. Shahnas, Department of Physics, University of Toronto, 60 St. George St., Toronto, ON M5S 1A7, Canada. (peltier@atmosp.physics.utoronto.ca; shahnas@atmosp.physics.utoronto.ca)